FACTORS AFFECTING THE EFFICIENCY OF A WET TYPE DUST COLLECTOR

by

ROBERT EARL STEWART
B.E., Nova Scotia Technical College, 1957

A THESIS SUBMITTED IN PARTIAL FULFILMENT OF THE REQUIREMENTS FOR THE DEGREE OF

MASTER OF APPLIED SCIENCE

in the Department

of

Mechanical Engineering

We accept this thesis as conforming to the required standard

THE UNIVERSITY OF BRITISH COLUMBIA

August, 1963

In presenting this thesis in partial fulfilment of the requirements for an advanced degree at the University of British Columbia, I agree that the Library shall make it freely available for reference and study. I further agree that permission for extensive copying of this thesis for scholarly purposes may be granted by the Head of my Department or by his representative. It is understood that copying or publication of this thesis for financial gain shall not be allowed without my written permission.

Department of Mechanical Engineering,
The University of British Columbia,
Vancouver 8, British Columbia,
Canada.

August, 1963

ABSTRACT

Performance tests on a wet type dust collector were made using four different test dusts to determine a relationship between dust collection efficiency, particle size and size-distribution, collector nozzle velocity, and collector geometry. Dust laden air entered the collector and impinged upon a water surface at nozzle velocities in the order of 10,000 fpm. The fraction of dust which penetrated the collector was found to fit the equation

$$\pi = 233\ \phi_g^{2.61} \cdot V^{-0.939} \cdot J^{0.146}$$

where

π = collector penetration (100% minus efficiency)

ϕ_g = Geometric Coefficient of Variation of the test dust

$$= \frac{\text{Geometric Standard Deviation}}{\text{Geometric Mean Diameter}}$$

V = collector nozzle velocity in thousands of fpm

$$J = \frac{\text{length of jet throw to mean water level}}{\text{nozzle throat dimension}}$$

π was found to vary from 0.121 percent with Corundum dust to 8.68 percent with Alundum dust. The nozzle velocity range was from 6840 fpm to 14,130 fpm and the range of J was from 6.85 to 27.4. Corundum dust was found to have a value of ϕ_g equal to 0.123 with a geometric mean diamter, $\bar{d}_g$, of 11.9 microns while ϕ_g and $\bar{d}_g$ for Alundum were calculated to be 0.521 and 4.84 microns respectively. The four test dusts were sized by a sedimentation method.

The Function equation fits the experimental results with an uncertainty of $\pm$ 12 percent.

ACKNOWLEDGEMENTS

I am indebted to Dr. J.L. Wighton for the design of the dust collector and his many helpful suggestions on the presentation of the material; and to Mr. E. Abell for his help and suggestions in constructing the apparatus.

I also wish to thank the National Research Council of Canada who helped finance the project under NRC Grant A 881.

TABLE OF CONTENTS

LIST OF FIGURES

LIST OF TABLES

LETTER SYMBOLS

a	length of jet throw; acceleration; radius
A	area; asymmetry parameter
d	particle diameter
$\bar{d}$	arithmetic mean diameter
$\bar{d}_g$	geometric mean diameter
D	drag force; abbreviation for dust
D_o	orifice diameter
f,F	function; force
g	acceleration of gravity
G	apparent specific gravity
h	height
J	dimensionless ratio pertaining to dust collector geometry = $\frac{a}{\delta}$
k	constant
K	constant; flow coefficient
m	mass; mode
M	median
n	sample size
P	pressure
q	velocity component
Q	weight flow rate
r	radius
R	gas constant; coordinate
Re	Reynolds number
s	standard deviation

s_g geometric standard deviation

S skewness parameter

t time

T temperature

u velocity component in the x-direction

U,V velocity

v specific volume; velocity component in the y-direction

w accumulated weight falling full height of suspension in time t

W accumulated weight deposited in time t

w velocity component in the z-direction

Y expansion factor

GREEK LETTERS

α temperature correction factor

γ specific weight

δ nozzle throat dimension

θ angle

μ dynamic viscosity

π collector penetration; 3.1416

ρ mass density

Σ summation

σ error

σ^2 variance

τ shear stress

ϕ coefficient of variation

∇ vector operator del

SUBSCRIPTS

a	dry air
D	dust type
f	fluid
g	geometric
i	number
j	collector geometry
m	mixture
n	nozzle
θ	angle
p	pressure; particle
r	radius
R	coordinate
s	shear
sv	saturated vapor
v	vapor
V	nozzle velocity
w	water column

INTRODUCTION

Although various types of dust collection equipment have been in industrial use for many years, their operation is still not fully understood. It is very difficult to predict accurately the performance of dust collectors and any new approach to the problem is a welcome one. The dust collector dealt with in this presentation could be classified as a scrubber. It was designed solely for the purpose of investigating some of the more important variables which influence dust collector performance. The variables investigated were the collector geometry, collector nozzle velocity, and various properties of the test dusts. A factorial plan was used to investigate the effect of these variables on collector penetration, and this approach is explained in Chapter 3. Simple statistical tests are used throughout the presentation as a means of revealing the significance of the data, as well as determining the error in the function relation. The discussion of particle sizing by sedimentation has been confined entirely to Chapter 2 to avoid confusion on the reader's part since the subject appears to be separated from the problem investigated.

CHAPTER 1

1.1 DUST COLLECTION THEORY

Dusts can be formed by nature or they can be formed by mechanical processes such as the reduction of larger masses by crushing and grinding.

The performance of a dust collector is usually expressed in terms of collection efficiency and is computed as the weight ratio of dust collected to dust entering the collector. Another way of expressing collector performance, called the penetration, is the weight ratio of the dust not collected in the collector to the weight of dust entering the collector. The penetration, π , is equal to 100 percent minus the efficiency. The wet type dust collector used in this presentation was designed to trap suspended solids in a scrubbing liquid, usually water. The dust-laden air stream is passed through a nozzle to form a high velocity jet which impings vertically upon a water surface. The air forms a trough, see Fig. 1.4, penetrating some distance below the mean water level, makes a small-radius 180 degree bend and escapes from the collector. The dust particles, because of their greater inertia, tend to be collected by the water. The air in the trough sets up a spray action above the liquid, a wave motion on the water surface, and a circulation of water through the entire water bath causing thorough mixing of the solids in the liquid. The scrubbing action of the trough and the water droplets formed, tend to increase efficiency.

The wetting characteristics of the liquid do not necessarily play a major role in the actual process of dust collection, although wetting agents may serve to avoid re-entrainment of dust particles once they

have been impinged on liquid droplets. (10)

Some scrubbers are not very effective in collecting particles finer than about 5 microns, or 0.005 mm. The more effective scrubbers will collect particles of about 1 or 2 microns but penetration increases rapidly for finer particles (10).

Probably the most important variables influencing collector penetration for the dust collector used in this presentation are the properties of the dust such as size distribution, shape, density; and the velocity of the dust-laden air at contact with the liquid surface. It is this jet velocity which determines the intensity of the scrubbing action and the formation of water droplets.

It is easily seen that penetration should decrease with increases in jet velocity and/or particle size.

1.2 DUST COLLECTION APPARATUS

Figure 1.1 is a flow diagram of the dust collection apparatus. Compressed air at approximately 80°F and 75 psig is reduced in pressure, passed through a tank containing water, and then metered. Some of the clean humidified air is then bled through a dust feeder which provides the dust-laden air to be cleaned in the collector. Dust which penetrates the collector is passed through an air sampler containing a paper filter. The dust feeder and the paper filter are weighed before and after a run so as to determine the penetration.

Figure 1.2 shows a view of the dust collector and the air sampler. The dust feeder is shown in Figure 1.3. Figure 1.4 gives some indication of the extent of the scrubbing action and water droplet formation taking place in the collector.

During operation, a small amount of clean water was continuously added to replace dirty water carrying solids to waste. The water level in the collector was controlled by adjusting the primary weir, weir A. The pressure in the collector was balanced by a secondary weir, weir B. The collector itself was constructed out of plexiglass with a removable front for cleaning and changing nozzles. The overall nominal dimensions of the collector were 28" high by 9" wide and 2" deep.

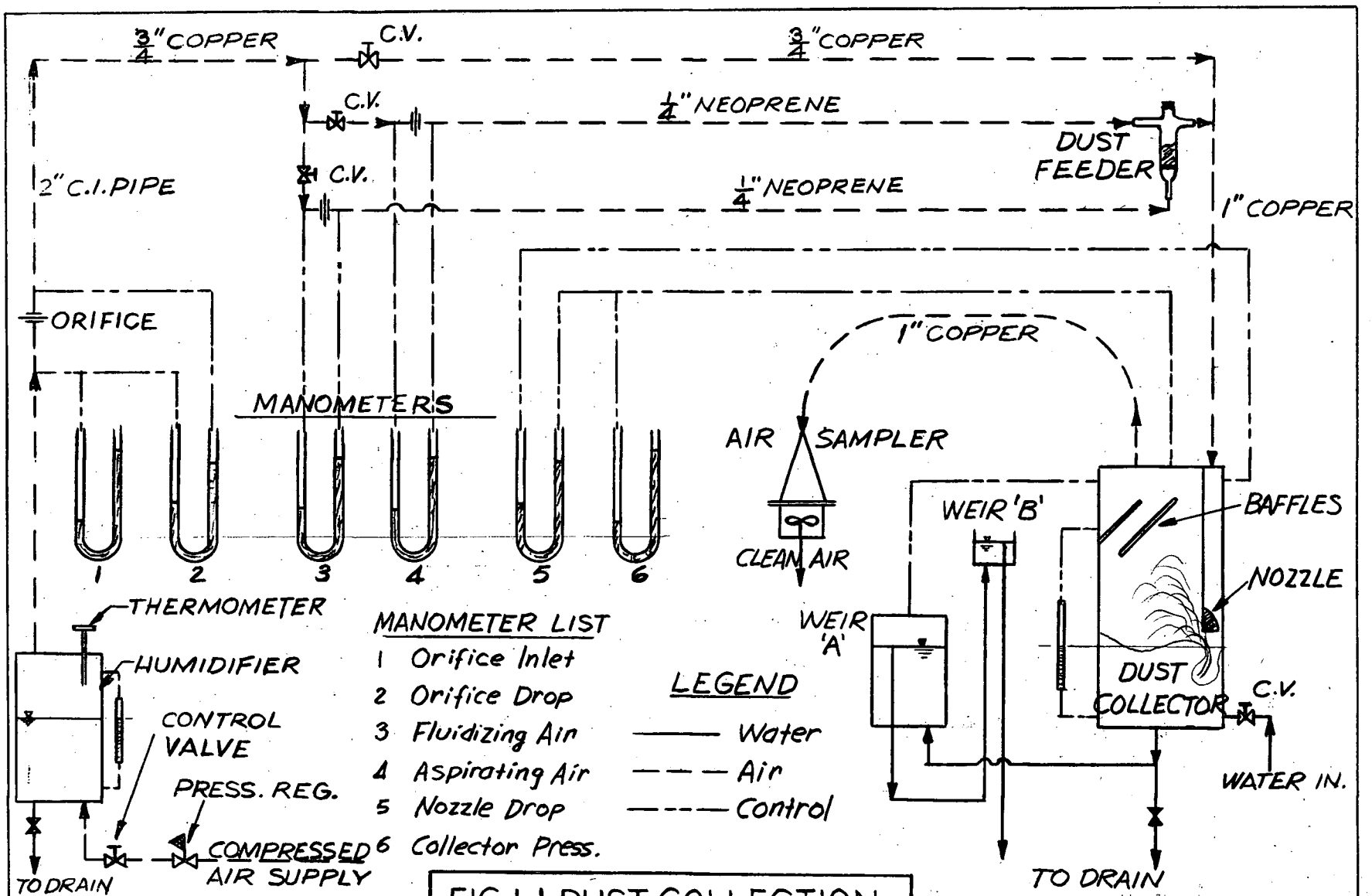

FIG. 1-1 DUST COLLECTION FLOW DIAGRAM

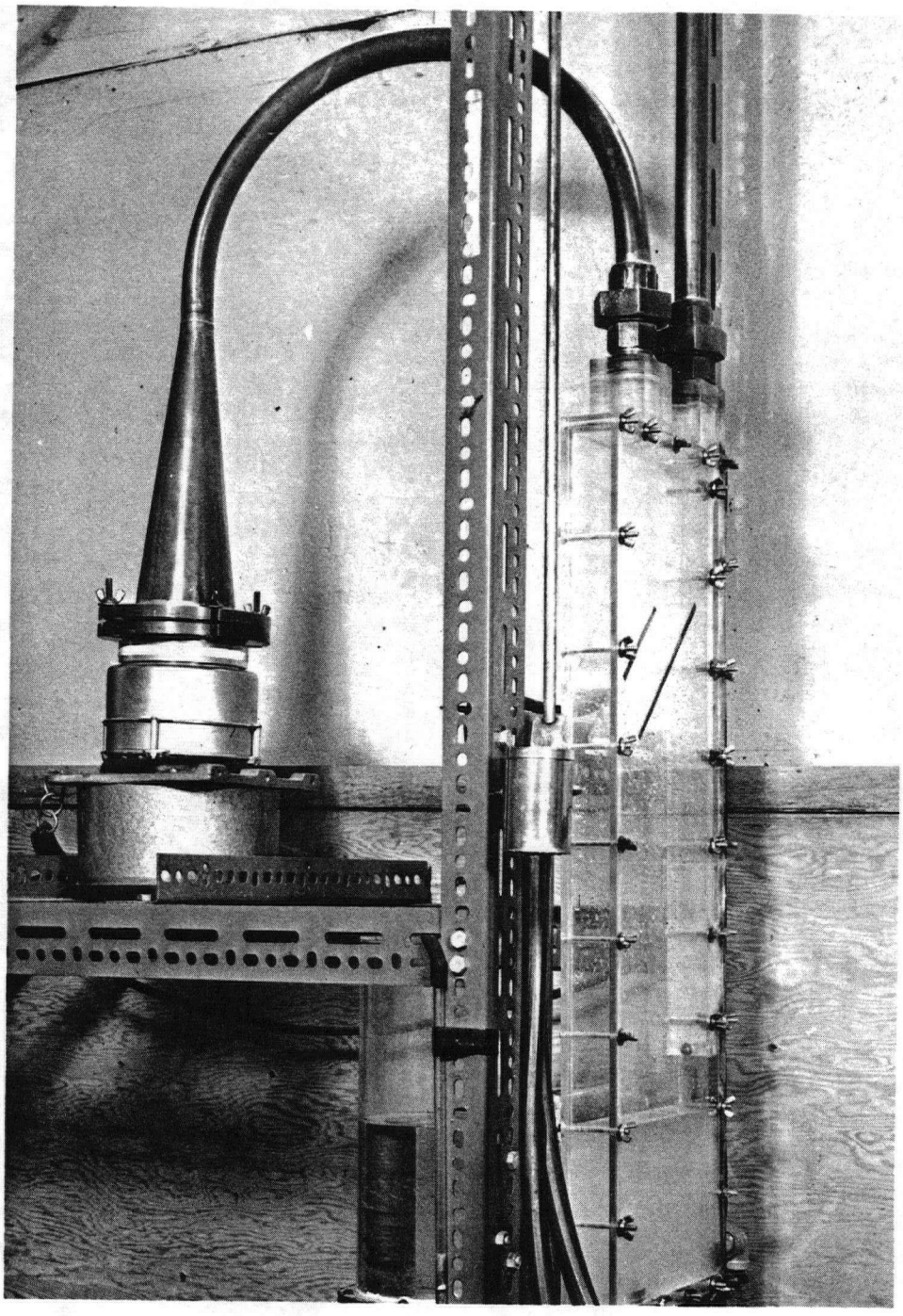

FIGURE 1.2 PHOTOGRAPH OF DUST COLLECTOR AND FILTER HOLDER

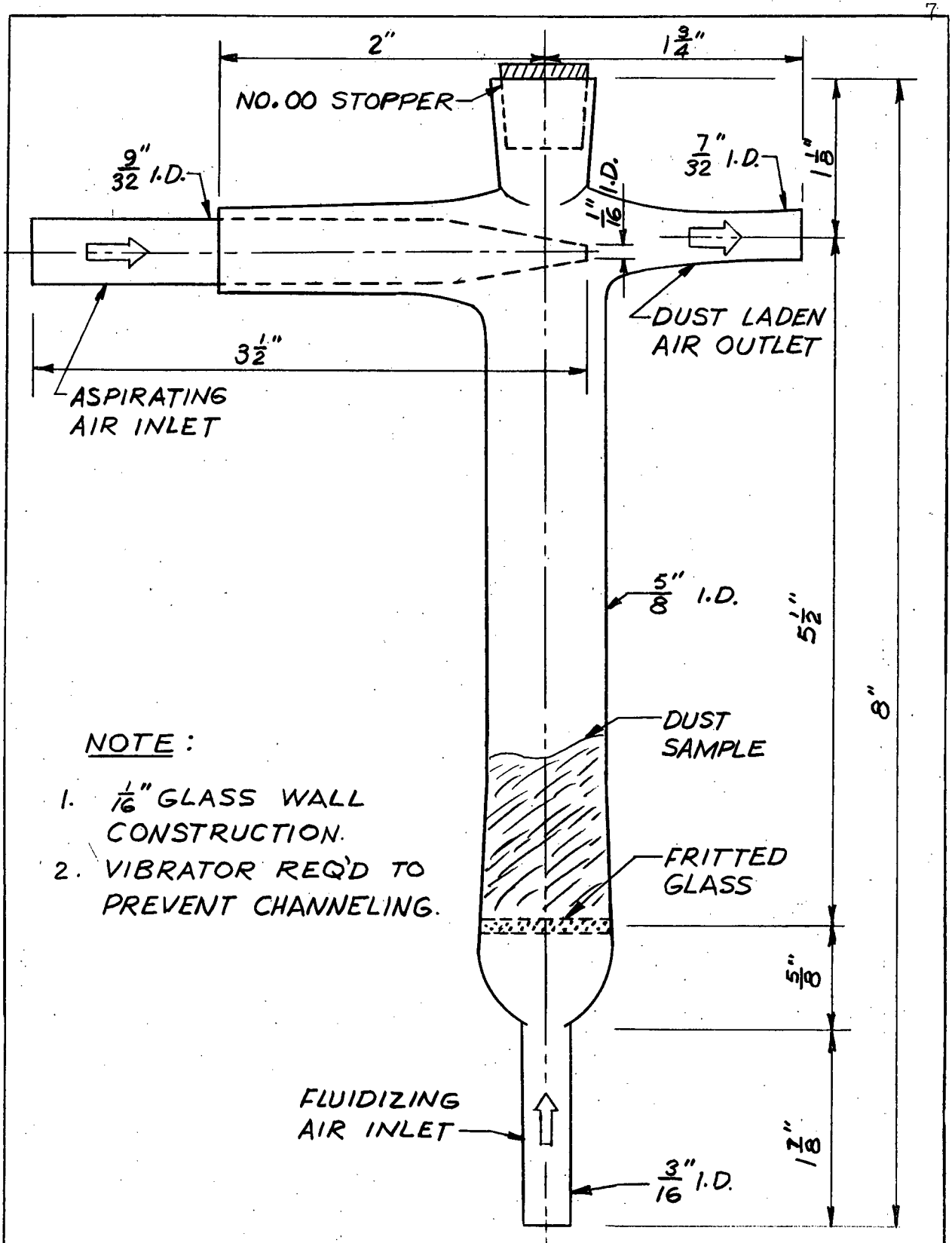

FIG. 1·3 DUST FEEDER

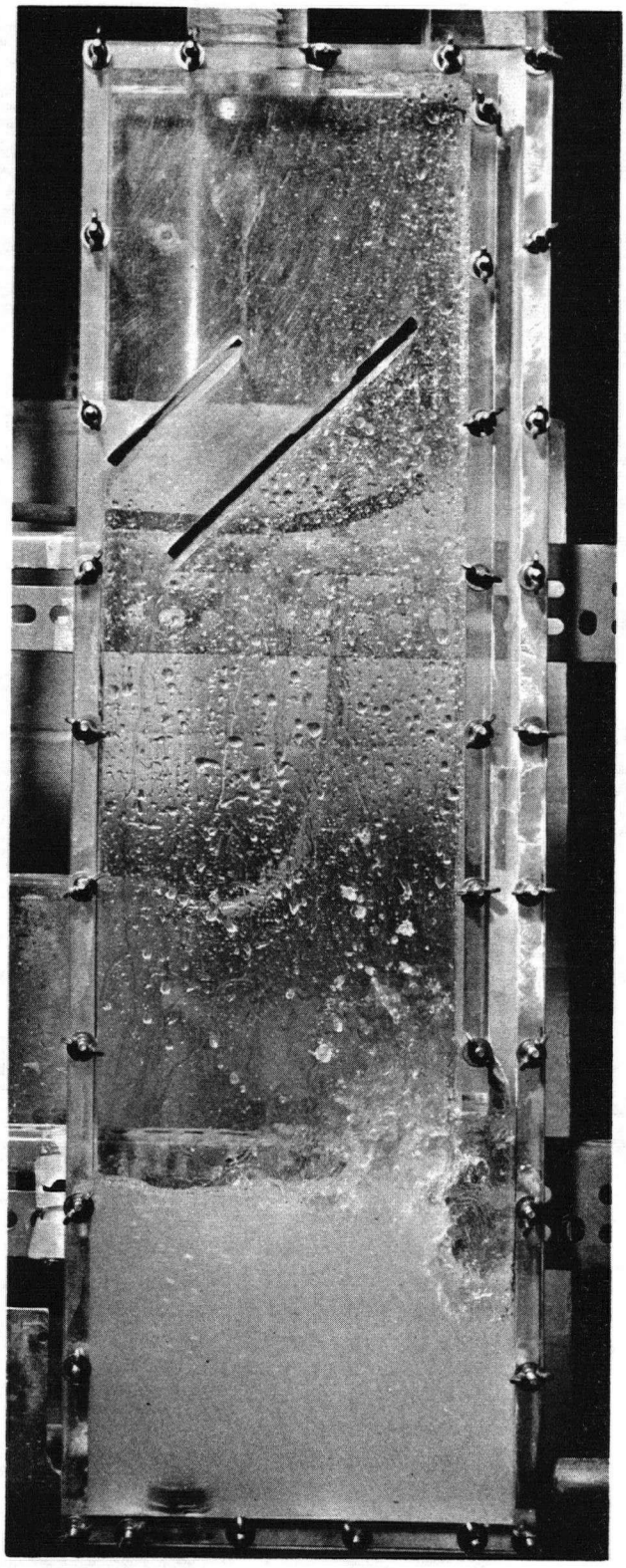

FIGURE 1.4 PHOTOGRAPH OF SCRUBBING ACTION

Collector Geometry, J

Figure 1.5 shows the collector nozzle configuration. The depth of the nozzle passage is 1.47" and the radius of curvature of the nozzle is approximately 4". The parameter used to describe the collector geometry is given by

$$J = \frac{a}{\delta} \qquad \text{where}$$

a = length of jet throw from nozzle discharge to mean water level

δ = nozzle throat dimension = 0.109"

The variable 'a' was changed by adjusting the water level in the collector. For this experiment, the range of 'a' chosen was from 1" to 3" so that the range of J was from 6.85 to 27.4.

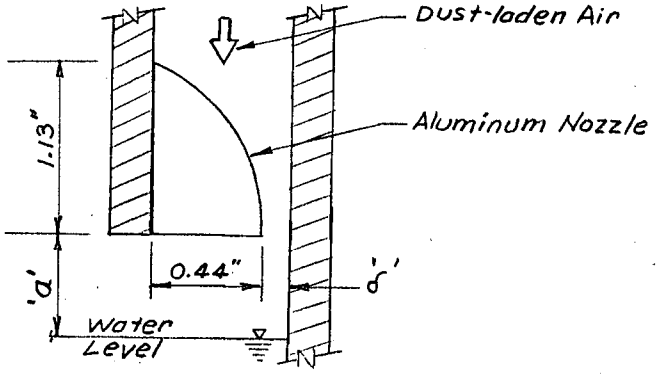

A_n = Nozzle throat Area
= 1.47 δ

Figure 1.5 Collector Nozzle Detail

Nozzle Velocity, V

The jet or nozzle velocity used in the correlation was found by first calculating the quantity of air through the orifice.

The amount of air supplied to the collector was determined from the orifice equation (18)

$$Q = 359.1\ KYD_o\alpha\sqrt{\gamma_1 h_w} \quad \text{lbs./hr.} \qquad (1.1a)$$

where K = flow coefficient

Y = expansion factor

D_o = orifice diameter, inches

α = temperature correction factor

γ_1 = specific weight of air at orifice inlet, lb/ft^3

h_w = orifice drop, in w.c.

For $D_o = 0.520$ inches

$K = 0.725$

$\alpha = 1.00$

$Y = 1.00$

equation (1.1a) became

$$Q = 70.5\sqrt{\gamma_1 h_w} \quad \text{lb/hr.} \qquad (1.1b)$$

or

$$Q = 1.18\sqrt{\gamma_1 h_w} \quad \text{lb/min.} \qquad (1.1c)$$

Substituting the continuity equation between the orifice and the collector nozzle, Equation (1.1c) becomes

$$\gamma_n A_n V_n = 1.18\sqrt{\gamma_1 h_w} \quad \text{lb/min.} \qquad (1.2)$$

where γ_n = specific weight of air at nozzle throat, lb/ft^3

A_n = area of nozzle throat, ft^2

V_n = velocity of air at nozzle throat, ft/min.

The nozzle velocity then is

$$V_n = \frac{1.18}{A_n} \frac{\sqrt{\gamma_1 h_w}}{\gamma_n} \quad \text{ft/min.} \qquad (1.3)$$

For $A_n = 0.161\ in^2$

then $$V_n = 1054 \frac{\sqrt{\gamma_1 h_w}}{\gamma_n} \quad \text{ft/min.} \qquad (1.4)$$

Since we are dealing with a mixture of air and water, humidity must be considered in calculating γ_1 and γ_n. The relative humidity of the air leaving the humidifier is assumed to be 80% (16). The temperature of the air for all runs was $69 \pm 1^{\circ}F$.

The specific weight of the mixture was

$$\gamma_m = \gamma_a + \gamma_v \qquad (1.5)$$

where

$$\gamma_V = \text{R.H.} \times \gamma_{s.v.}$$

$$= 0.001 \ lb/ft^3$$

and

$$\gamma_a = \frac{144(P-Pv)}{R\,T}$$

and

γ_m = specific weight of mixture, lb/ft^3

γ_a = specific weight of dry air, lb/ft^3

γ_v = specific weight of vapor, lb/ft^3

$\gamma_{s.v.}$ = specific weight of saturated vapor, $\frac{1}{896}$ lb/ft^3

P_V = vapor pressure, 0.351 psia.

R.H. = relative humidity, 0.80

R = gas constant, 53.3 $\frac{\text{ft. lb.}}{\text{lb. }^{\circ}\text{R}}$

T = temperature $^{\circ}$R, 529

γ_n in Equation (1.4) is assumed equal to the specific weight of the air in the collector, downstream of the nozzle, and both γ, and γ_n in Equation (1.4) can be found from Equation (1.5).

The nozzle velocity V used in the investigation is given by Equation (1.4). The velocity range selected was from 6840 to 14,130 fpm. This velocity range was the maximum that could be obtained without having to readjust any of the valves, except the supply air valve, shown in the flow diagram, Figure 1.1.

The fluidizing air and aspirating air for the dust feeder were adjusted by manually operated control valves to provide the proper amount of feeder air for the dust samples. This is indicated by manometers 3 and 4, Figure 1.1. The air sampler contains a suction fan, whose static pressure can be adjusted to compensate exactly for the increase in pressure drop caused by the build up of dust on the filter paper. Thus the back pressure in the collector is maintained constant throughout a run.

Collector Penetration, π

The most critical part of the experiment is the actual calculation of the penetration itself. For dusts having very low penetrations, the amount collected on the filter may be so small that a change in moisture content of the filter paper may result in an appreciable error in determining the penetration.

The paper filters used were found to change their weight by as much as 2 mg. under ideal test conditions.

The weighing procedure was as follows:

(i) the filters were placed in weighing bottles and oven dried for three hours at 250°F;

(ii) the filters were then removed from the oven and placed in a dessicator jar where they were cooled to room temperature and then weighed;

(iii) after a dust collector run, the filter used was put through (i) and (ii) until no change in weight was observed.

An alternative approach, that of igniting the filter after a run and weighing the residue to determine the penetration, could have been used but it was felt that the ignition might affect the dust so that a true weight would not be obtained.

In summary, then, all dust collector runs were made at predetermined nozzle velocities and collector water levels. All runs making up an experiment were repeated under the same operating conditions but not in the same sequence. Different sample sizes were used in the second set of runs.

CHAPTER 2

2.1 PARTICLE SIZE DETERMINATION

Since a correlation of collector penetration with particle-size and size distribution as well as nozzle velocity and collector water level is to be attempted, it is necessary to find a suitable means for sizing the particles.

The characteristics of a single particle are seldom of interest, but the mean characteristics of a large collection of particles enable the sample to be identified. These mean characteristics or statistical measures are calculated from data obtained by the measurement method chosen. The most widely used unit of particle size is the micron.

$$1 \text{ micron} = 0.001 \text{ mm} = 10^{-4} \text{ cm.}$$

$$= \frac{1}{25{,}400} \text{ in.}$$

The term 'particle size' generally refers to the average or equivalent diameter of a particle. The particles used in this text are of the sub-sieve range, approximately less than 50 microns.

The following approximate values assist in formulating a physical concept of such fine particles. (1)

Table 2.1 Scale of Magnitudes

Diameter of large molecules	0.005 microns
Wavelength of visible light	0.5 "
Atmospheric dust	0.5 "
Talcum powder	2-20 "
Limit of vision with unaided eye	10-40 "

Flour	10-100 microns
Diameter of human hair	50-200 "

The dust samples were sized by a liquid sedimentation method, in which an initially homogeneous dispersion was allowed to settle out onto a balance pan. The total weight sedimented was automatically recorded as a function of time. Then the size distribution was obtained from the slopes of the weight versus time curve and Stokes law.

Stokes Law for Falling Spheres

Sedimentation techniques depend on Stokes law of resistance for a sphere falling with zero acceleration in a fluid. The resistance law is developed in Appendix A. It can be written as

$$D = \frac{3\pi}{g} \mu V d \qquad (2.1)$$

where g = acceleration due to gravity, $\frac{cm}{sec^2}$

D = drag force due to pressure and shear, gm.

μ = dynamic viscosity of fluid, $\frac{gm}{cm.sec.}$ or Poise

V = velocity of the falling sphere, cm/sec.

d = diameter of the sphere, cm.

The drag term in Equation (2.1) can be eliminated to make the equation more usable.

Consider one dimensional vertical motion of a sphere of diameter d, density ρ_p, and volume v having zero acceleration in a fluid of viscosity μ and density ρ_f.

Then,

$$\sum F = v(\rho_p - \rho_f) - D = ma = 0$$

and

$$D = \frac{\pi d^3}{6} (\rho_p - \rho_f) \quad gm$$

Substituting Equation (2.2) in Equation (2.1) and simplifying, then

$$d^2 = \frac{18\mu}{(\rho_p - \rho_f)g} \cdot V \qquad (2.3)$$

If the sphere falls a height h cm. in time t minutes then the diameter of the sphere in microns is given by

$$d = 175 \sqrt{\frac{\mu}{\rho_p - \rho_f} \cdot \frac{h}{t}}, \quad \text{microns} \qquad (2.4)$$

Equation (2.4) is a convenient form of Stokes law for determining the diameters of freely falling spheres having zero acceleration in a stationary fluid.

Limitations on Stokes Law

Equation (2.1) has been derived under the important assumption that inertia terms in the Navier-Stokes equations can be neglected. The law is only approximate even for very low values of Reynolds number since

$$Re = \frac{\text{Inertia Forces}}{\text{Viscous Forces}} = \frac{\rho_f dV}{\mu} \qquad (2.5)$$

The error in velocity due to inertia forces being present has been estimated by Davies (8). He estimated that values of Re corresponding to error of 1, 5, and 10 percent in the velocities of settling spherical particles are 0.074, 0.38, and 0.82. A maximum Reynolds number of 0.3 was used in the present work, so the maximum error in velocity was about 4 percent. The particle diameter corresponding to a maximum Reynolds number of 0.3 is calculated below.

From Equations (2.3) and (2.5) we obtain

$$d^3 = \frac{18\mu^2}{\rho_f(\rho_p - \rho_f)g} \cdot Re \qquad (2.6a)$$

which can be written as

$$d^3 = \frac{18\mu^2}{\rho_f^2(G-1)g} \cdot Re \qquad (2.6b)$$

where G is the specific gravity of the particles.

The allowable diameter corresponding to a maximum $R_e = 0.3$ for spheres settling in water at 20°C is

$$d_{max} = 10^4 \left[\frac{18(0.0105)^2}{1(G-1)980}\right]^{1/3} \text{ microns}$$

$$= \frac{85}{(G-1)^{1/3}} \text{ for } R_e = 0.3 \qquad (2.7)$$

On the other hand, when the particles are small compared to the mean free path of the molecules in the medium surrounding them, there is a tendency for the particles to slip between the spaces not occupied by the molecules. Correction factors made by Stokes-Cunningham are applied to particles smaller than 0.1 microns settling in air at standard conditions (4).

Heywood (14) gives the normal lower limit of particle diameter determined by gravitational sedimentation as 2 microns and with careful temperature control particles can be sized down as find as 1 micron. In this presentation, a 2 micron lower limit is used.

Stokes law does not account for interference effects between particles and from the walls of the sedimenting vessel since it applies only to particles falling in a medium of unlimited extent. Careful

tests (13) have shown that for dust concentration not greater than 1% by volume the errors due to particle interference and the walls of the container are negligible.

Particle Density, Medium Density and Viscosity

The particle density, ρ_p , was calculated as follows (16).

A pycnometer flask was weighed several times; (i) empty; (ii) partly filled with test dust; and (iii) with the test dust and sufficient distilled water to fill the calibrated flask to the etched line on the neck. Before final weighing, the mixture was dispersed, brought slowly to a boil to eliminate air bubbles, and cooled to the temperature at which the pycnometer was calibrated. The weights of the dust and water were found by difference. The difference between the water volume and the contained volume was the sample volume from which the specific gravity or density could be determined. The procedure was repeated for all the test dusts and the results checked against data from the manufacturers and handbooks.

Distilled water was used as the sedimentation medium. Values of density and viscosity for distilled water at various temperatures are shown in Figure 2.1.

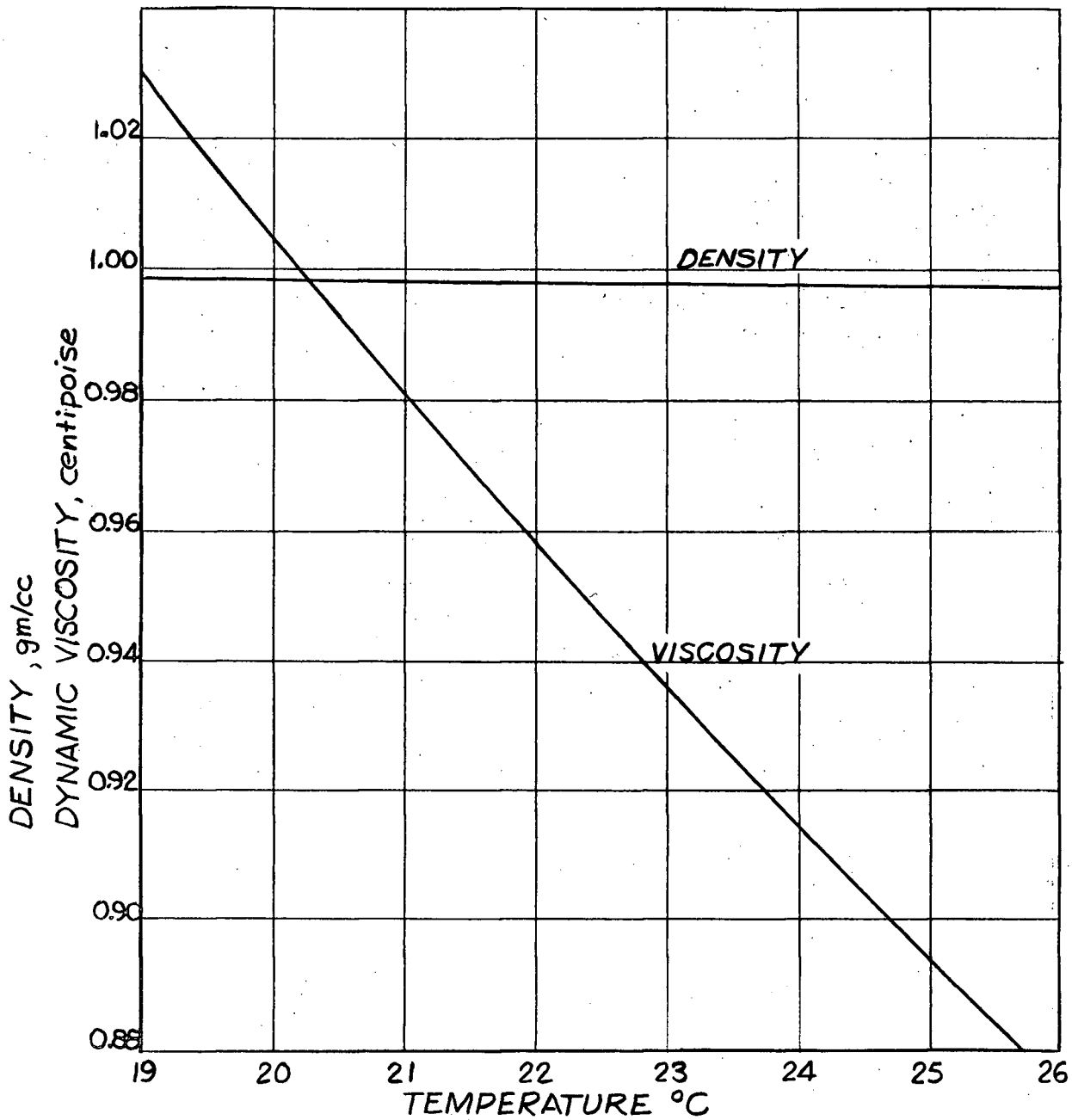

FIG. 2-1 DENSITY AND VISCOSITY OF DISTILLED WATER

2.3.2 SEDIMENTATION METHOD AND APPARATUS

Figure 2.2 is a photograph of the complete sedimentation apparatus. In operation, a sample of the test dust is thoroughly dispersed in the sedimentation column. At the bottom of the column a pan is suspended from the beam of an electronic recording balance. The weight of dust deposited on the pan causes the balance beam to deflect. In so doing more light is directed onto a photo-cell which sends a signal to a motor. The motor transmits a restoring force to the balance beam. At the same time the recorder pan is moved to a new position on the paper. The paper moves at a constant speed and an accumulated weight versus time curve is obtained.

Any desired amount of dust up to 1.5 grams can be used. The sensitivity of the balance is far greater than that required for this particular application.

In setting up the sedimentation process;

(i) The sedimentation chamber is filled to a desired level with distilled water to which has been added 2 grams/litre of Calgon dispersing agent, which tends to prevent coagulation.

(ii) About 75 cc of the sedimentation medium is added to approximately 0.25 cc of test dust in a weighing bottle, the bottle and dust having been weighed to the nearest mg.

(iii) The mixture is thoroughly dispersed and placed in a vacuum tank to remove any air bubbles.

(iv) The dispersed solution is then quickly poured into the sedimentation column and is stirred at the same time. The recording trace is quite noisy during the first 5 or 10 seconds.

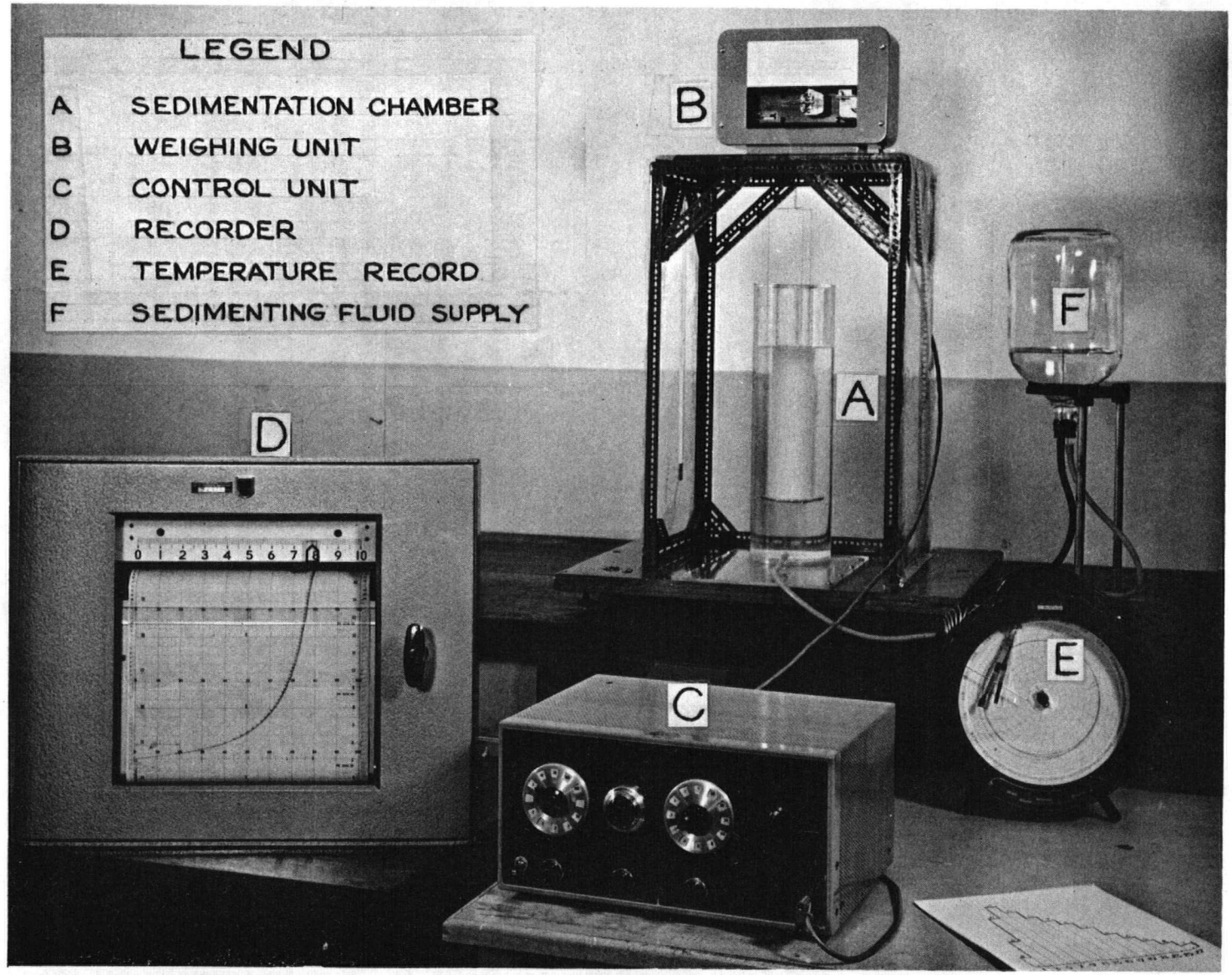

FIGURE 2.2 PHOTOGRAPH OF SEDIMENTATION APPARATUS

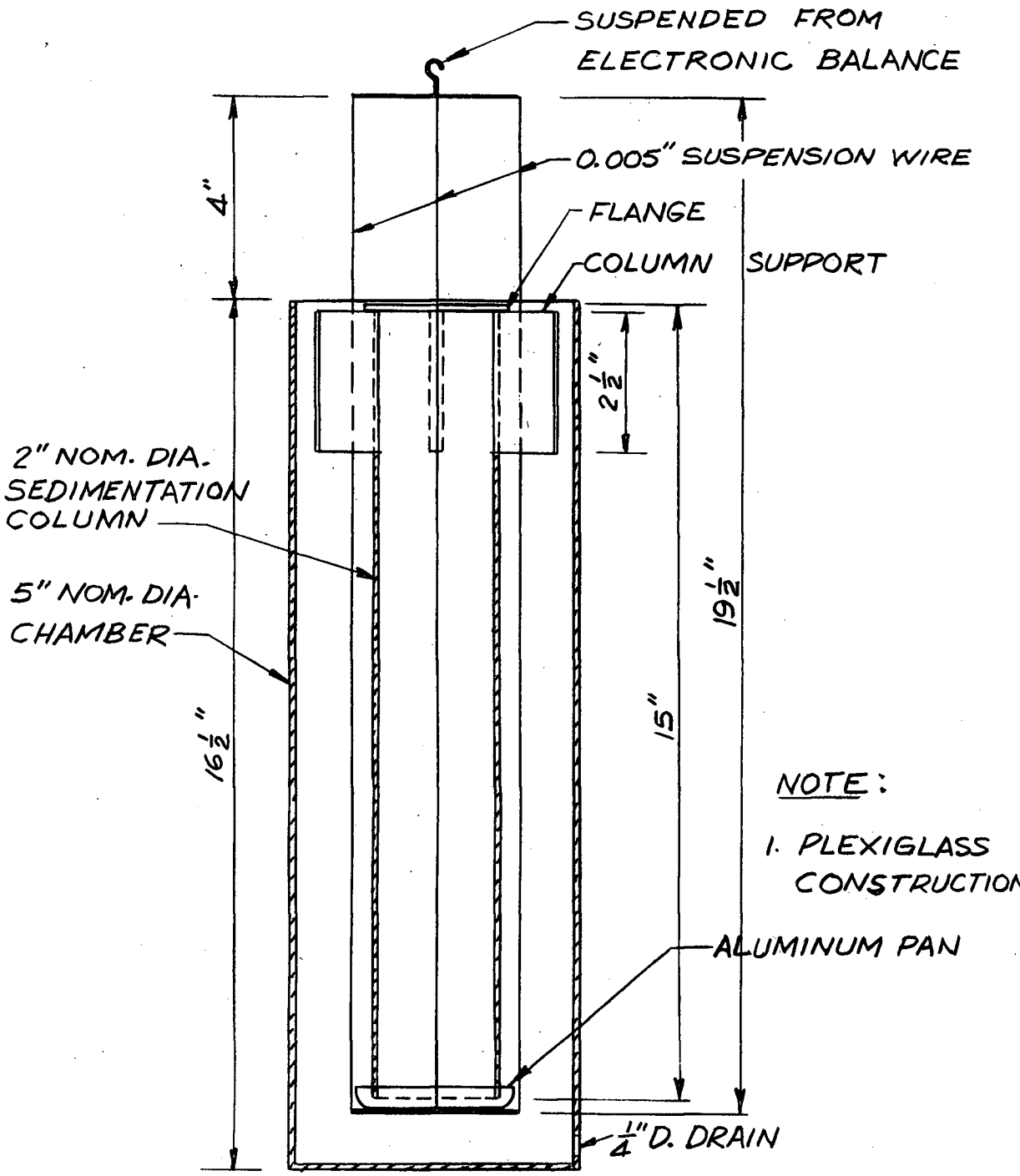

FIG.2·3 SEDIMENTATION CHAMBER

(v) The weighing bottle is oven-dried, cooled to room temperature and re-weighed.

The amount of dust placed into the sedimentation column is then determined by differencing the weighings taken in (ii) and (v) above.

The temperature of the air surrounding the sedimentation chamber is maintained to within $\pm$ 1°C by means of a thermostat controlled room air conditioner.

A drawing of the sedimentation chamber is shown in Figure 2.3.

The solid material which settles on the pan in time t is made up of two fractions; (i) one fraction having particles with a time of fall less than t and whose size is therefore greater than that specified by t; (ii) a fraction containing smaller particles with a longer time of fall than t but which have fallen in t since they were below the full sedimenting height. Oden (11,12) has shown that this second fraction is equal to $t\left(\frac{dW}{dt}\right)$ where W is the percent cumulative weight deposited in time t and dW and dt are differentials.

The first fraction, mentioned above, w, represents the whole of the fraction of the material of size greater than, or equal to, that size which would just fall the full height of the suspension in the time t.

The basic equation is:

$$W = w + t\left(\frac{dW}{dt}\right) \qquad (2.8a)$$

which is conveniently written as

$$w = W - \frac{dW}{d(\ln t)} \qquad (2.8b)$$

The curve of accumulated weight deposited versus time, obtained by the electronic recording-balance is replotted in the form: percentage weight deposited, W versus the natural log of the time $\ln t$, for t in seconds.

$\frac{dW}{d(\ln t)}$ can then be obtained by graphical differentiation of the curve at appropriate values of t and the desired fraction, w can be found by use of Equation (2.8b).

In the present work a simplified method due to Bostock (12) was used. It involves the drawing of tangents at convenient values of $\ln t$. The corresponding w is equal to the intercept made by the tangent on the ordinate at $\ln t - 1$. The proof is as follows:

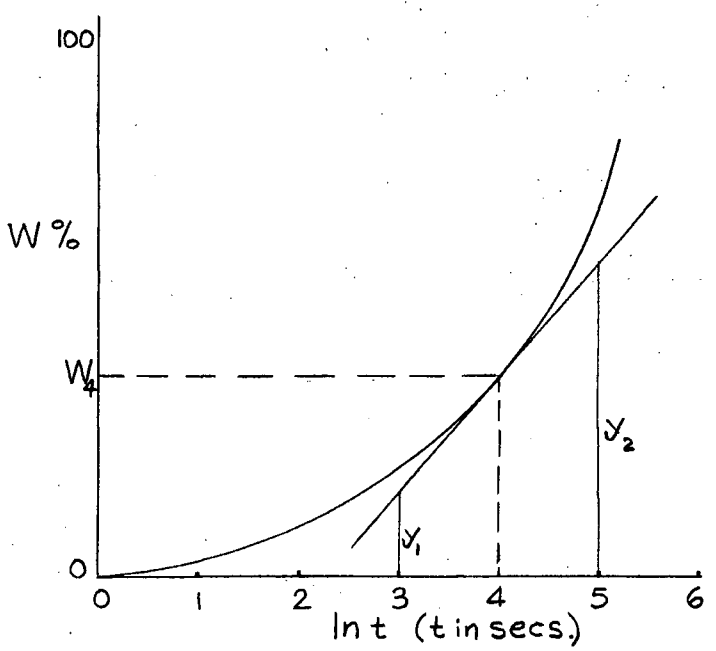

Figure 2.4 Determination of Size Fraction, w%

With reference to Figure 2.4, the slope at W_4 is $\frac{y_2-y_1}{2}$ which equals $\frac{dW_4}{d(\ln t)}$ and $W_4 = y_1 + \frac{1}{2}(y_2-y_1)$.

Substituting into Equation (2.8b), then $w_4 = y_1 + \frac{1}{2}(y_2-y_1) - \frac{y_2-y_1}{2}$ or $w_4 = y_1$.

The values of w thus obtained were plotted against the equivalent spherical diameter determined by equation (2.4).

The values of t chosen to determine w and d are given by

$$t_i = \sqrt{2}\,(t_i-1)$$

beginning with t_3 where t_1 and t_2 were chosen to be $\frac{1}{4}$ and $\frac{1}{2}$ minutes respectively.

From the resulting size-distribution curve (w versus d) the size-frequency curve which gives the amount of w in given size ranges, was drawn.

Various statistical measures were then determined.

A list of the statistical measures which were determined from the size-distribution and size-frequency curves for the four dusts used in the experiment are: arithmetic mean; standard deviation; median; 25% quartiles; mode; asymmetry; inter-quartile range; 5%-95% range; skewness parameter; coefficient of variation; geometric mean; geometric standard deviation; geometric coefficient of variation.

A detailed description of these properties is given in Appendix B.

The sedimentation procedure was carried out for the four test dusts used. Each of the four sedimentation runs was replicated once, using sample sizes, sedimentation heights and sedimentation medium temperatures different from those used in the first set of runs.

2.3 PARTICLE PROPERTIES

Tables 2.2 and 2.3 list values of accumulated weight deposited on the pan at various times. The data were taken directly from the recorder traces. Corresponding values of W are also given from which Figures 2.5 and 2.6 were drawn.

The curves of Figures 2.5 and 2.6 have little comparative meaning since the height of the sedimentation medium, the viscosity and the sample density differ from curve to curve.

The fraction w, in Equation (2.8b), was calculated. Tables 2.4 and 2.5 list w and the corresponding values of diameter as well as the test information necessary to calculate the diameters. Curves of w versus d are shown in Figures 2.7 and 2.8 for all test dusts.

The particle-size distribution curves, Figures 2.7 and 2.8, can also be presented in the form of particle-size versus frequency plots, or smoothed out histograms.

The histograms shown in Figures 2.9 and 2.10 were drawn so that the areas under each are identical.

A class interval of 1 micron was chosen for Corundum, for calculation of the mean and deviation, and a 2 micron class interval was chosen for the other three dusts.

Curves of w versus d for the first set of sedimentation runs were then plotted on log-probability paper, Figure 2.11. Since these curves are not linear, the size distributions are not quite log-normal so that a simple graphical method (Appendix B) for determining the geometric means and deviations cannot be used.

The histograms of Figure 2.12 show the actual distribution plotted on semi-log paper to show the deviations from the log-normal distributions.

TABLE 2.2. Cumulative Sedimented Weight vs. Time, First Set of Sedimentation Runs

Time t in min-secs	ln t (t in sec.)	CORUNDUM		BARITE		CALCIUM CARBONATE		ALUNDUM	
		Weight deposited mg.	W%	Weight deposited mg.	W%	Weight deposited mg.	W%	Weight deposited mg.	W%
0-15	2.71	7.6	1.48	13.9	4.18	4.6	0.94	6.5	1.73
0-30	3.40	15.3	2.96	27.8	8.35	9.15	1.87	13.5	3.59
0-42	3.75	21.7	4.19	38.9	11.7	12.8	2.61	20.8	5.53
1	4.10	30.5	5.89	55.5	16.7	18.3	3.74	29.3	7.8
1-25	4.44	43.3	8.36	77.8	23.4	25.6	5.22	34	9.05
2	4.79	61	11.9	105	31.5	36.6	7.47	39	10.4
2-50	5.13	86.5	16.9	129.5	38.9	51.2	10.5	45.3	12.06
4	5.48	122	23.6	150	45.0	72	14.7	52.5	14
5-40	5.82	173	33.4	171.5	51.5	97	19.8	59.3	15.8
8	6.17	244	47.1	193	58.0	124.5	25.4	69	18.4
11-20	6.51	312.5	60.4	212	63.7	154	31.4	81.3	21.6
16	6.87	380	73.3	229	68.8	187	38.2	98	26.1
22-40	7.20	429	82.8	244	73.3	220	44.9	121	32.2
32	7.55	467	90.2	258	77.5	251	51.2	150	39.9
45-20	7.89	491	94.9	271	81.4	282	57.5	185	49.2
64	8.25	504	97.2	280	84.1	309	63.0	220	58.5
90-40	8.59	509	98.1	289	86.8	330	67.4	254	67.5
128	8.94	513	99.0	296	89.0	345	70.5	281	74.7
181-20	9.29	-	-	303	91.0	354	72.3	305	81.1
256	9.64	-	-	307	92.2	-	-	322	85.6
326-40	9.99	-	-	-	-	-	-	335	89.1
∞	∞	518	100	333	100	490	100	376	100

TABLE 2.3. Cumulative Sedimented Weight vs. Time, Second Set of Sedimentation Runs

Time t in min-sec	ln t (t in sec.)	CORUNDUM		BARITE		CALCIUM CARBONATE		ALUNDUM	
		Weight deposited mg	W%	Weight deposited mg	W%	Weight deposited mg	W%	Weight deposited mg	W%
0-15	2.71	7.1	1.47	7.9	2.52	5.38	1.01	4.7	0.91
0-30	3.40	14.2	2.94	15.9	5.07	10.75	2.02	10.9	2.11
0-42	3.75	20.5	4.24	21.2	6.75	14.4	2.7	18.5	3.58
1	4.10	28.4	5.87	31.7	10.1	21.5	4.04	28.5	5.51
1-25	4.44	41	8.47	42.4	13.5	28.7	5.4	34.9	6.75
2	4.79	57	11.8	63.5	20.2	43	8.08	40.1	7.75
2-50	5.13	82	16.95	84.7	27	57.4	10.8	45.9	8.87
4	5.48	114	23.6	112	35.7	86	16.2	52.9	10.23
5-40	5.82	164	33.9	133	42.4	116.5	21.9	60.2	11.63
8	6.17	227	46.9	154.5	49.2	149	28	70.2	13.57
11-20	6.51	300.5	62.1	174.5	55.5	186.5	35	84	16.25
16	6.87	362	74.8	194	61.8	221	41.5	102.3	19.6
22-40	7.20	411	85	212	67.5	254	47.7	130.6	25.2
32	7.55	433.5	89.5	228	72.6	285	53.5	169	32.7
45-20	7.89	452.5	93.5	244	77.7	315	59.2	232	44.9
64	8.25	466	96.4	259	82.5	339	63.7	277	52.2
90-40	8.59	471	97.5	271	86.3	363	68.2	327	63.3
128	8.94	473	97.8	280	89.1	381	71.6	368.6	71.3
181-20	9.29	-	-	285.5	90.9	398	74.8	404	78.1
256	9.64	-	-	-	-	411	77.3	433.5	83.8
362-40	9.99	-	-	-	-	-	-	454.5	87.9
∞	∞	484	100	314	100	532	100	517	100

TABLE 2.4. PARTICLE-SIZE DISTRIBUTION, First Set of Sedimentation Runs

ln t (t in secs)	CORUNDUM		BARITE		CALCIUM CARBONATE		ALUNDUM	
	W%	d microns	W%	d microns	W%	d microns	W%	d microns
3								
3.5							0.8	69.5
4							2.5	54
4.5			2.8	36.9			4.3	42.2
5			15.4	28.6			6.5	32.8
5.5			26.8	22.4	1.2	35.3	8.3	25.5
6	2.0	21.1	37.1	17.4	6.5	28.0	9.8	19.9
6.5	20.6	16.4	47.8	13.6	12.6	21.9	10.4	15.5
7	48.9	12.8	57.3	10.5	21.9	17.0	10.4	12.1
7.5	72.1	9.9	65.8	8.2	31.5	13.3	16.1	9.4
8	88.7	7.8	73.2	6.4	43.1	10.3	25.0	7.3
8.5	94.9	6.0	79.2	5.0	55.0	8.1	40.1	5.7
9	98.1	4.7	84.0	3.9	64.5	6.3	57.3	4.4
9.5			88.0	3.0			71.1	3.5
10							80.7	2.7
Sample Density, gm/cc	3.85		4.50		2.71		3.58	
Water Temperature, °C	21.7		22.7		20.0		22.2	
Water Height, cm.	28.8		24.6		29.4		23.5	
Viscosity, centipoise	0.965		0.942		1.005		0.954	
Water Density, gm/cc	0.998		0.998		0.998		0.998	
Constant, K	423		349		564		399	

TABLE 2.5. PARTICLE SIZE DISTRIBUTION, Second Set of Sedimentation Runs

ln t (t in secs)	CORUNDUM		BARITE		CALCIUM CARBONATE		ALUNDUM	
	W%	d microns	W%	d microns	W%	d microns	W%	d microns
3.5							0.4	75
4							1.5	58.3
4.5							3.0	45.3
5			3.1	33.3			4.5	35.4
5.5	1.2	26.9	13.7	25.9	0.7	34.0	6.2	27.5
6	2.8	20.9	27.3	20.2	6.7	26.4	7.1	21.5
6.5	20.2	16.3	37.2	15.5	15.9	20.6	7.6	16.7
7	53.9	12.7	47.2	12.3	25.0	16.0	7.6	13.3
7.5	73.7	9.9	57.1	9.5	35.6	12.5	7.7	11.3
8	87.5	7.7	65.6	7.4	46.6	9.7	15.7	7.9
8.5	94.0	6.0	75.4	5.8	55.5	7.6	33.5	6.2
9	97.3	4.7	83.3	4.5	63.4	5.9	52.6	4.8
9.5					69.7	4.6	66.6	3.7
10							76.9	2.9
Sample Density, gm/cc	3.85		4.50		2.71		3.58	
Water Temp., °C	21.6		20.4		22.0		22.0	
Water Height, cm.	28.3		31.3		27.3		27.3	
Water Density, gm/cc	0.998		0.998		0.998		0.998	
Viscosity, centipoise	0.967		0.995		0.958		0.958	
Constant, K	420		405		530		431	

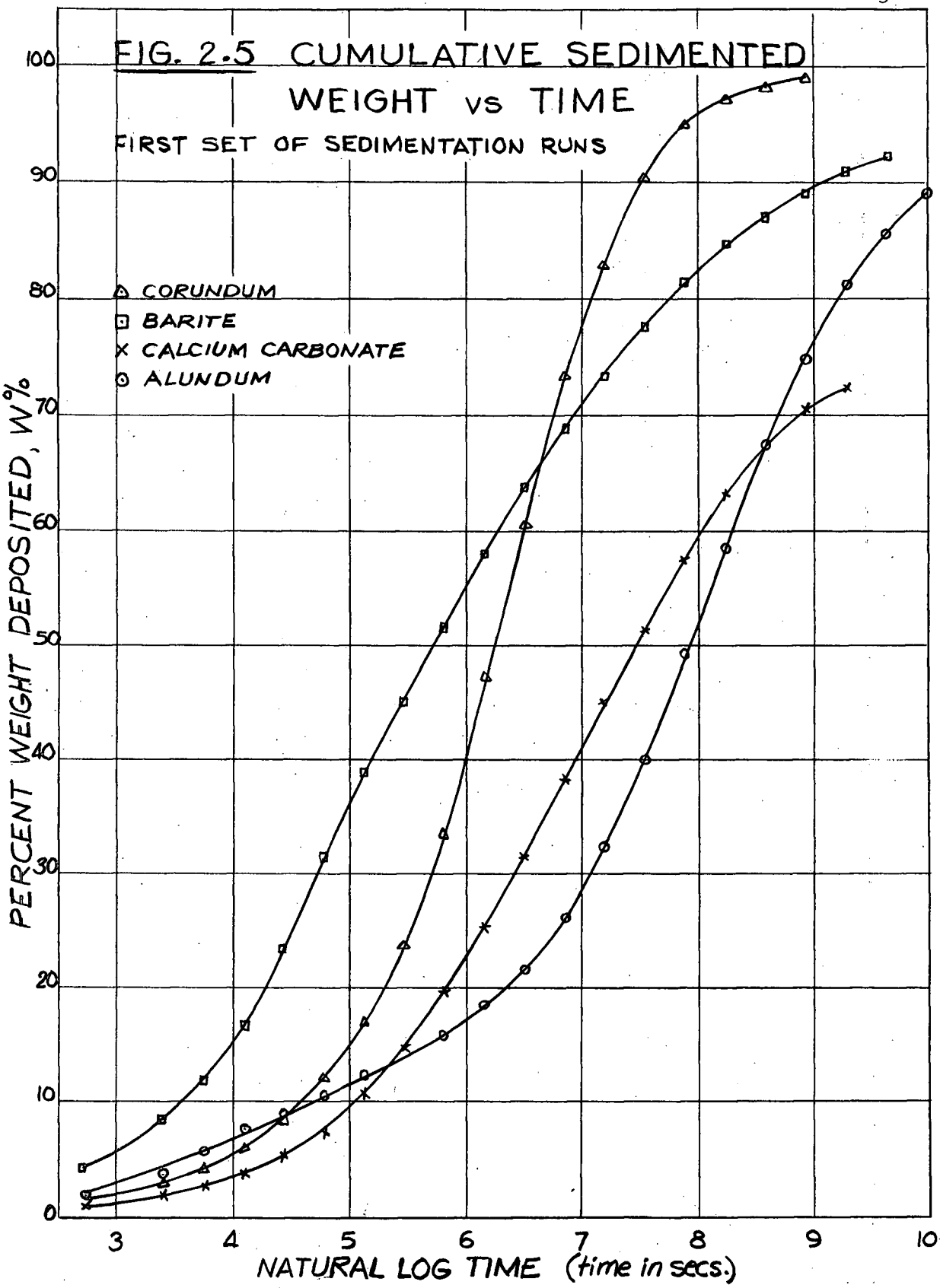
FIG. 2.5 CUMULATIVE SEDIMENTED WEIGHT vs TIME
FIRST SET OF SEDIMENTATION RUNS
CORUNDUM
BARITE
CALCIUM CARBONATE
ALUNDUM
PERCENT WEIGHT DEPOSITED, W%
0
10
20
30
40
50
60
70
80
90
100
3
4
5
6
7
8
9
10
NATURAL LOG TIME (time in secs.)

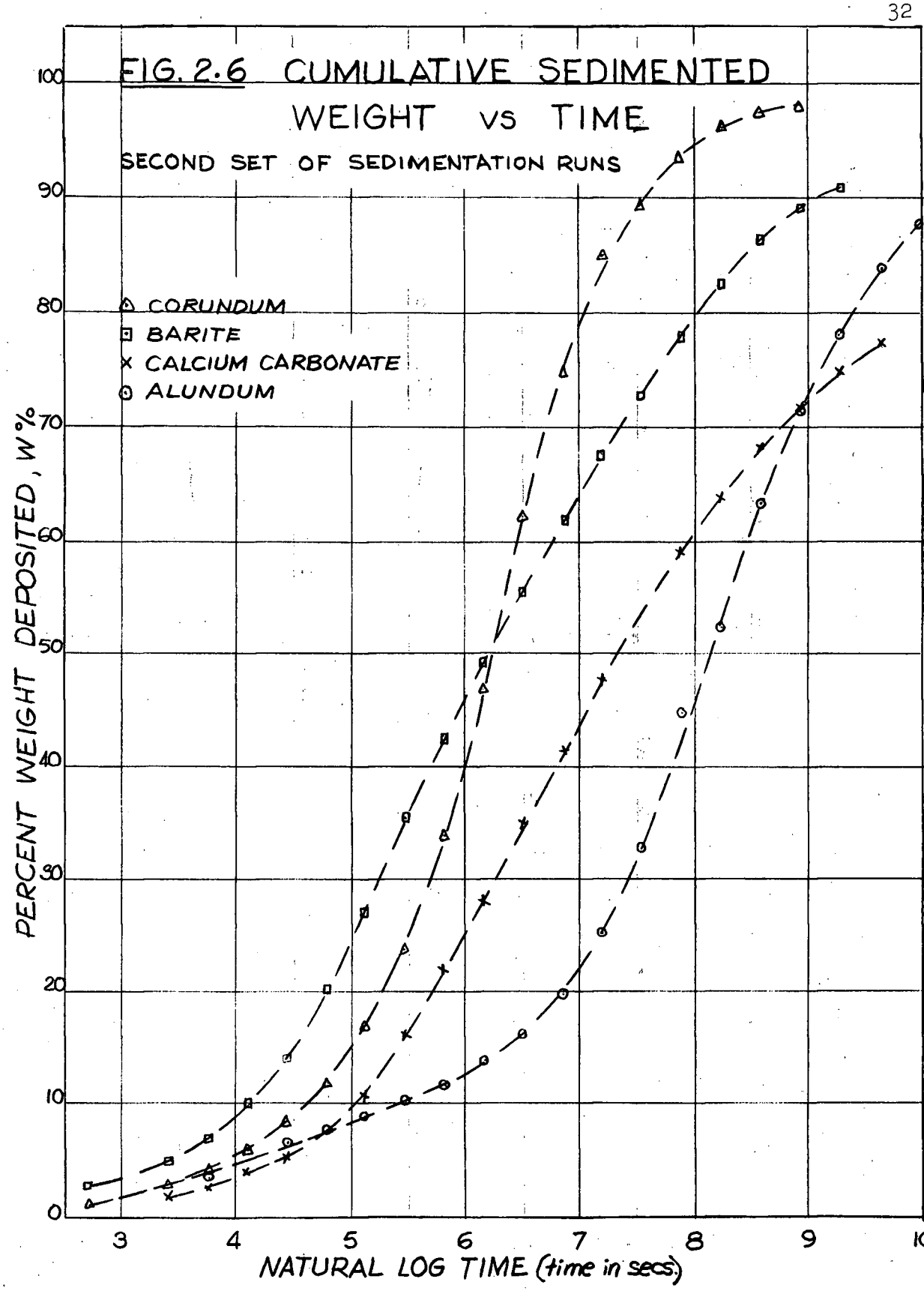
FIG. 2.6 CUMULATIVE SEDIMENTED WEIGHT VS TIME
SECOND SET OF SEDIMENTATION RUNS
CORUNDUM
BARITE
CALCIUM CARBONATE
ALUNDUM
PERCENT WEIGHT DEPOSITED, W%
0
10
20
30
40
50
60
70
80
90
100
3
4
5
6
7
8
9
10
NATURAL LOG TIME (time in secs)

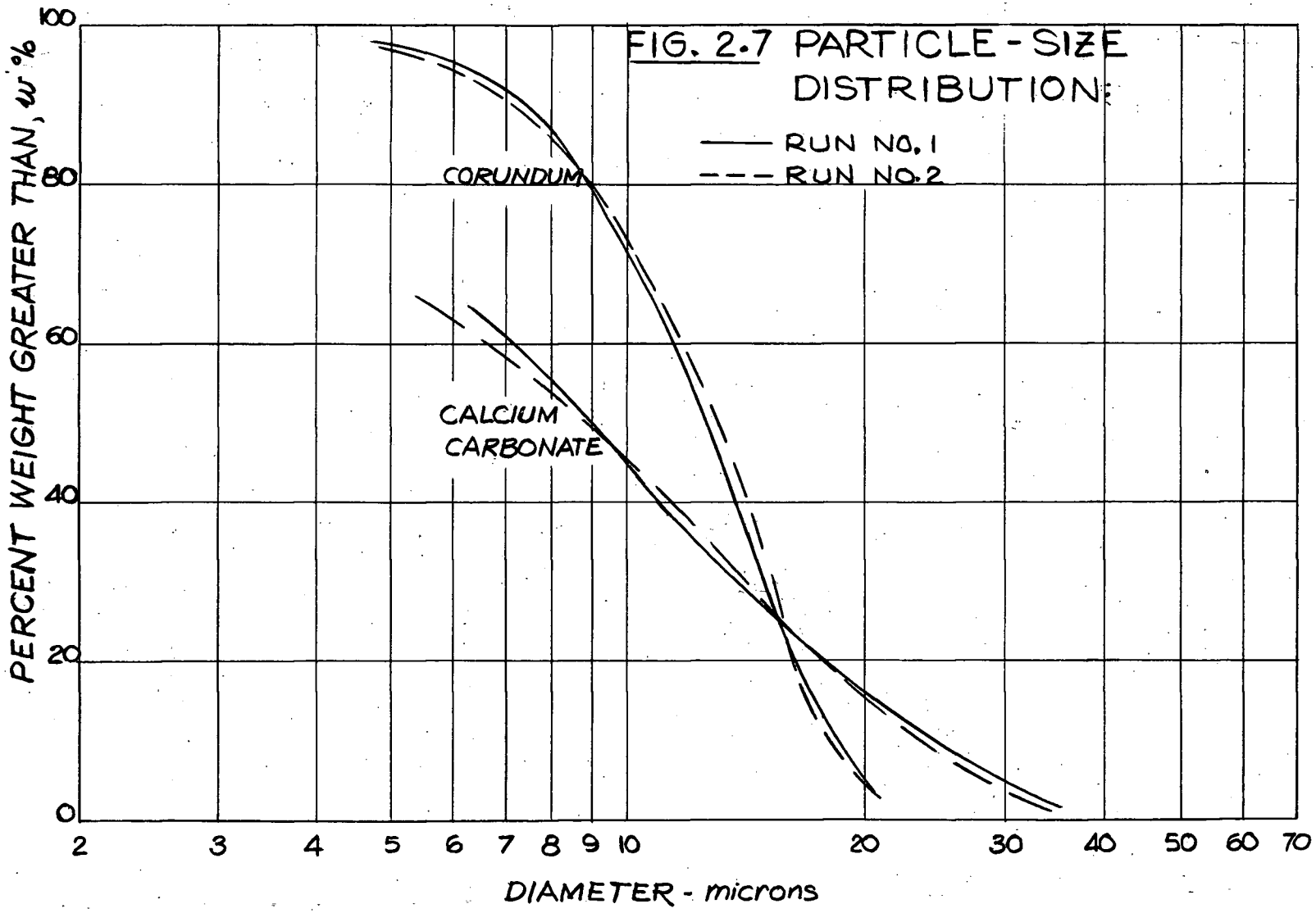
FIG. 2.7 PARTICLE-SIZE DISTRIBUTION
RUN NO. 1
RUN NO. 2
CORUNDUM
CALCIUM CARBONATE
PERCENT WEIGHT GREATER THAN, wt %
DIAMETER - microns
100
80
60
40
20
0
2
3
4
5
6
7
8
9
10
20
30
40
50
60
70

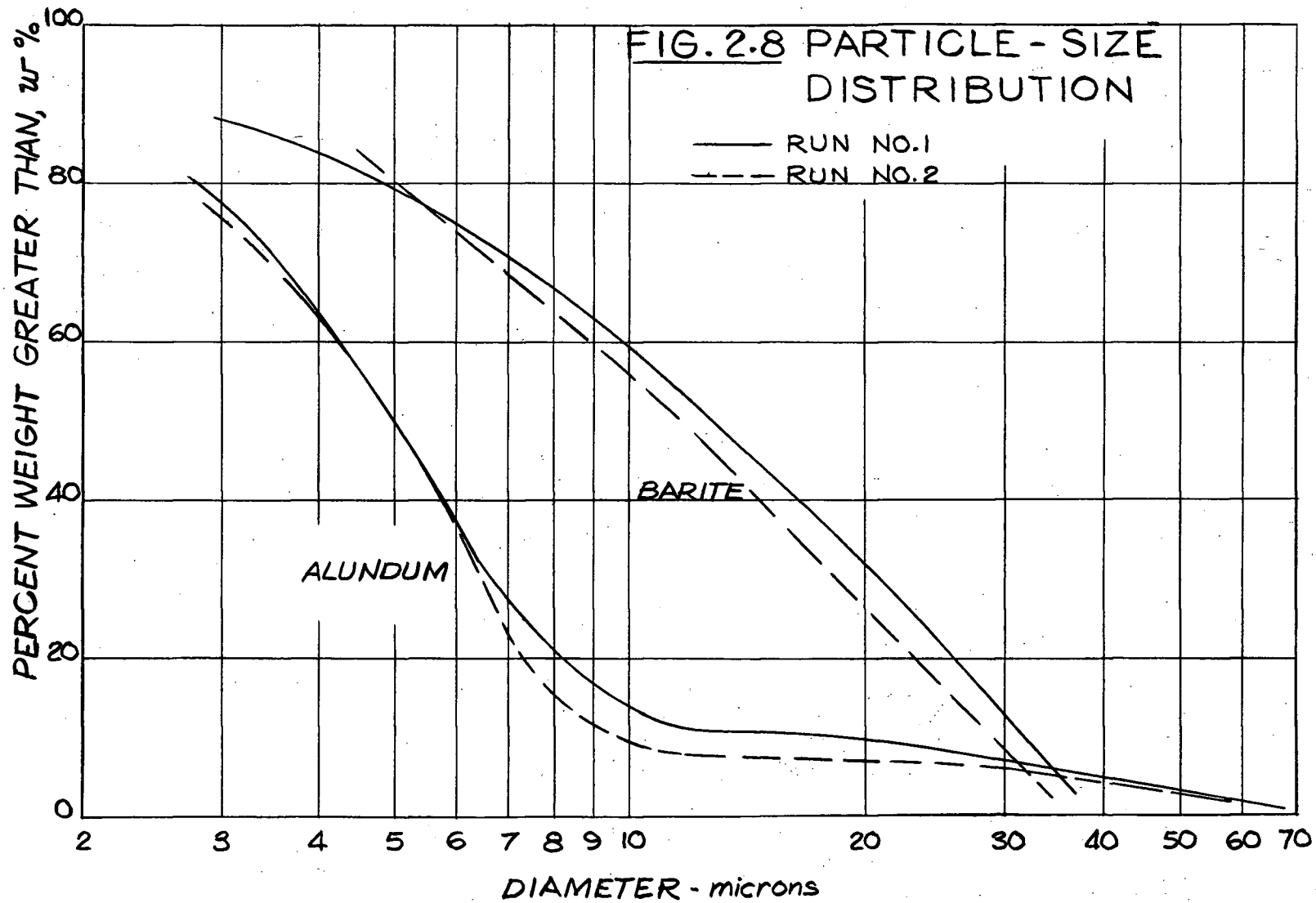
FIG. 2.8 PARTICLE-SIZE DISTRIBUTION
RUN NO.1
RUN NO.2
BARITE
ALUNDUM
PERCENT WEIGHT GREATER THAN, wt %
0
20
40
60
80
100
2
3
4
5
6
7
8
9
10
20
30
40
50
60
70
DIAMETER - microns

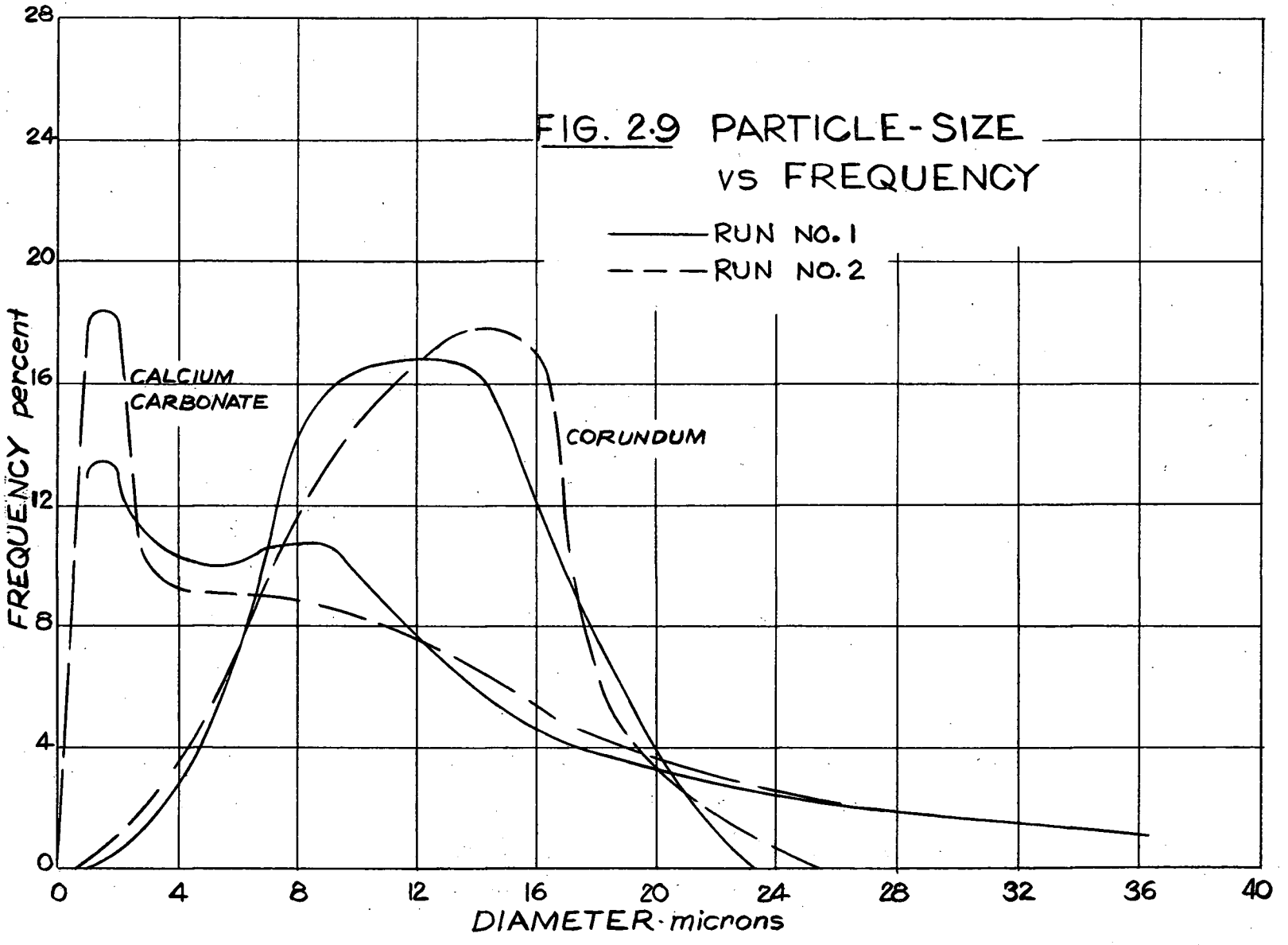
FIG. 2.9 PARTICLE-SIZE vs FREQUENCY
RUN NO. 1
RUN NO. 2
CALCIUM CARBONATE
CORUNDUM
FREQUENCY percent
DIAMETER · microns
0
4
8
12
16
20
24
28
32
36
40

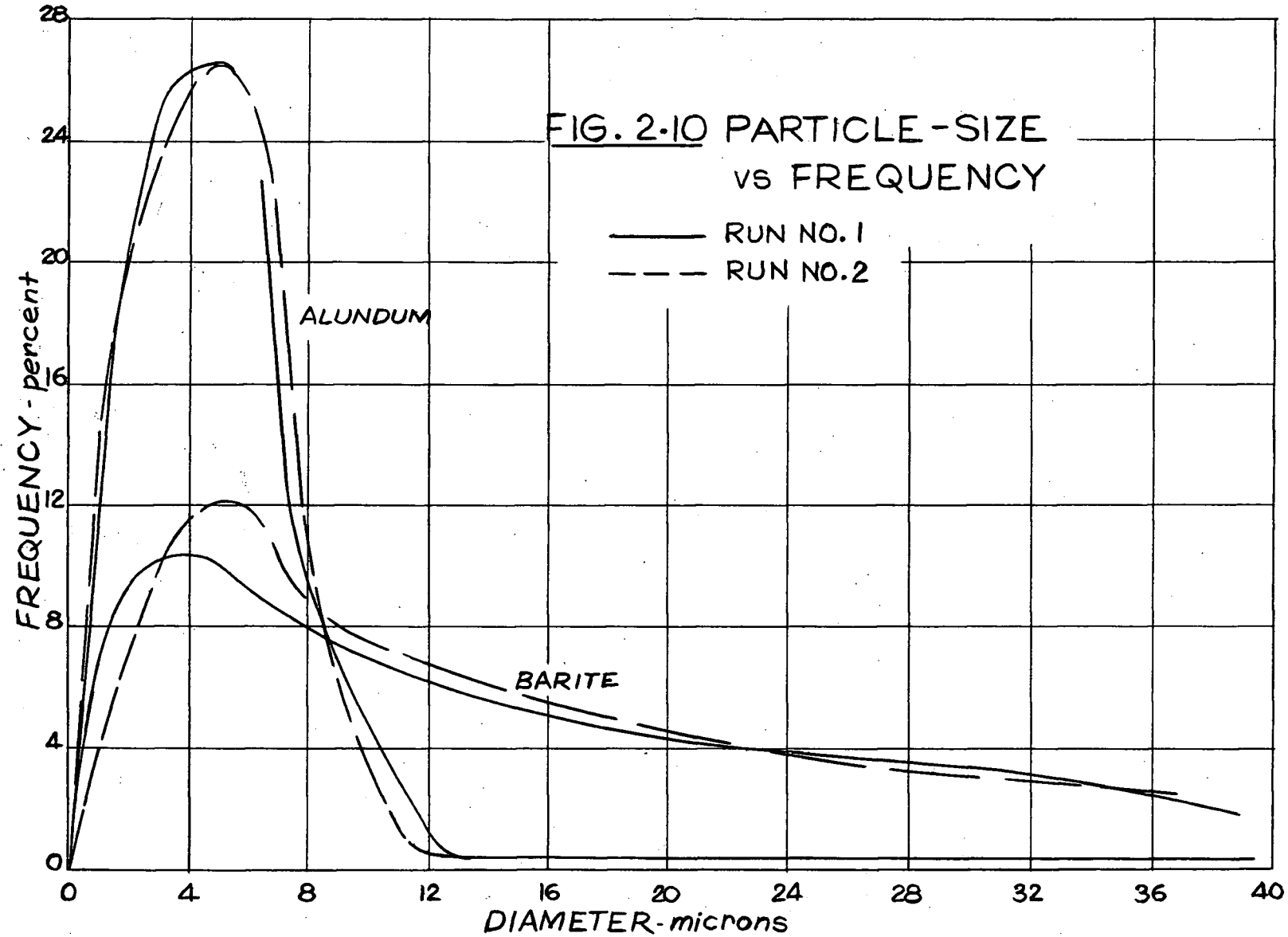
FIG. 2-10 PARTICLE-SIZE vs FREQUENCY
RUN NO. 1
RUN NO. 2
ALUNDUM
BARITE
FREQUENCY - percent
DIAMETER - microns
0
4
8
12
16
20
24
28
32
36
40

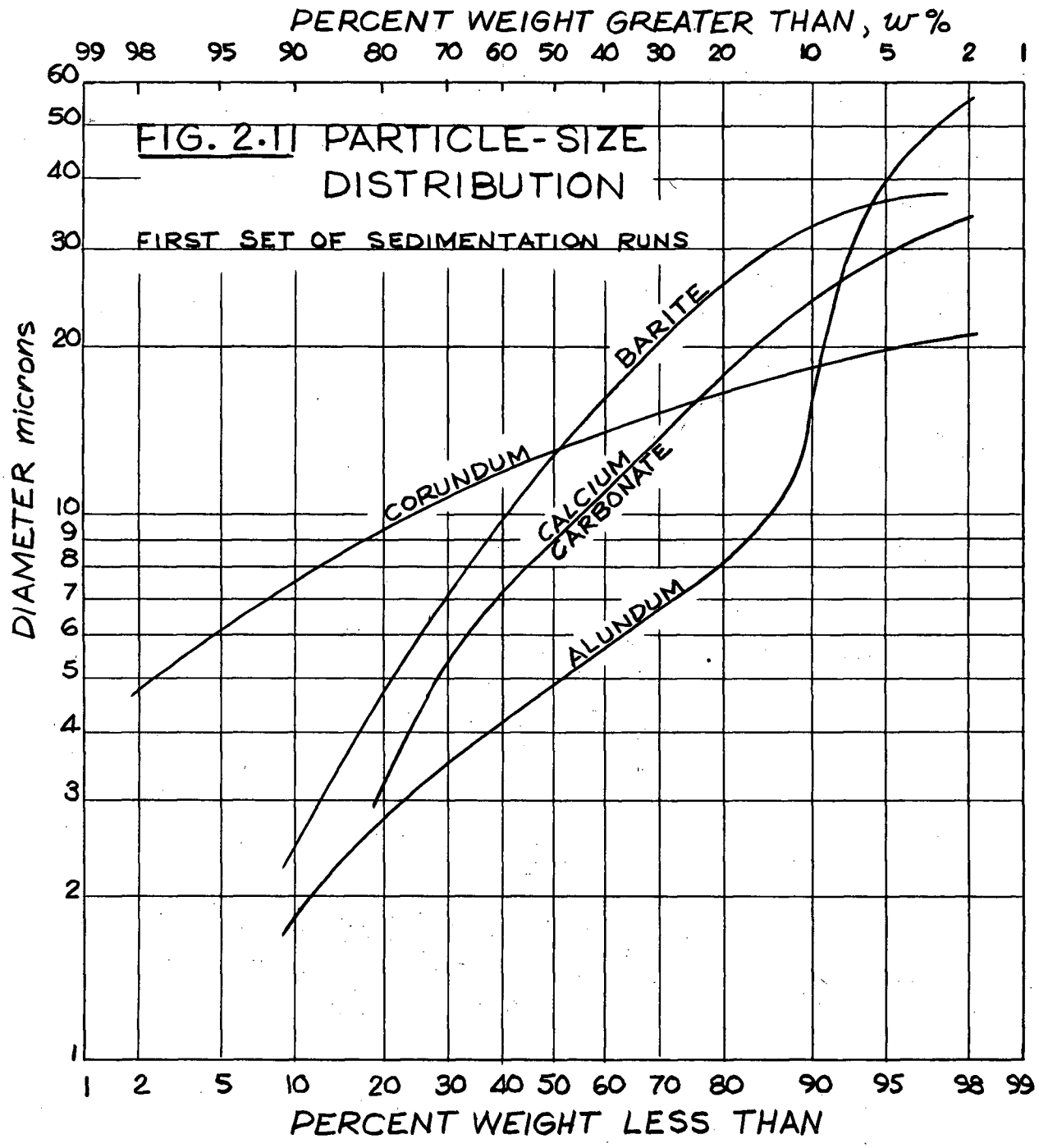
PERCENT WEIGHT GREATER THAN, w %
99 98 95 90 80 70 60 50 40 30 20 10 5 2 1
FIG. 2.11 PARTICLE-SIZE DISTRIBUTION
FIRST SET OF SEDIMENTATION RUNS
DIAMETER microns
60 50 40 30 20 10 9 8 7 6 5 4 3 2 1
BARITE
CORUNDUM
CALCIUM CARBONATE
ALUNDUM
1 2 5 10 20 30 40 50 60 70 80 90 95 98 99
PERCENT WEIGHT LESS THAN

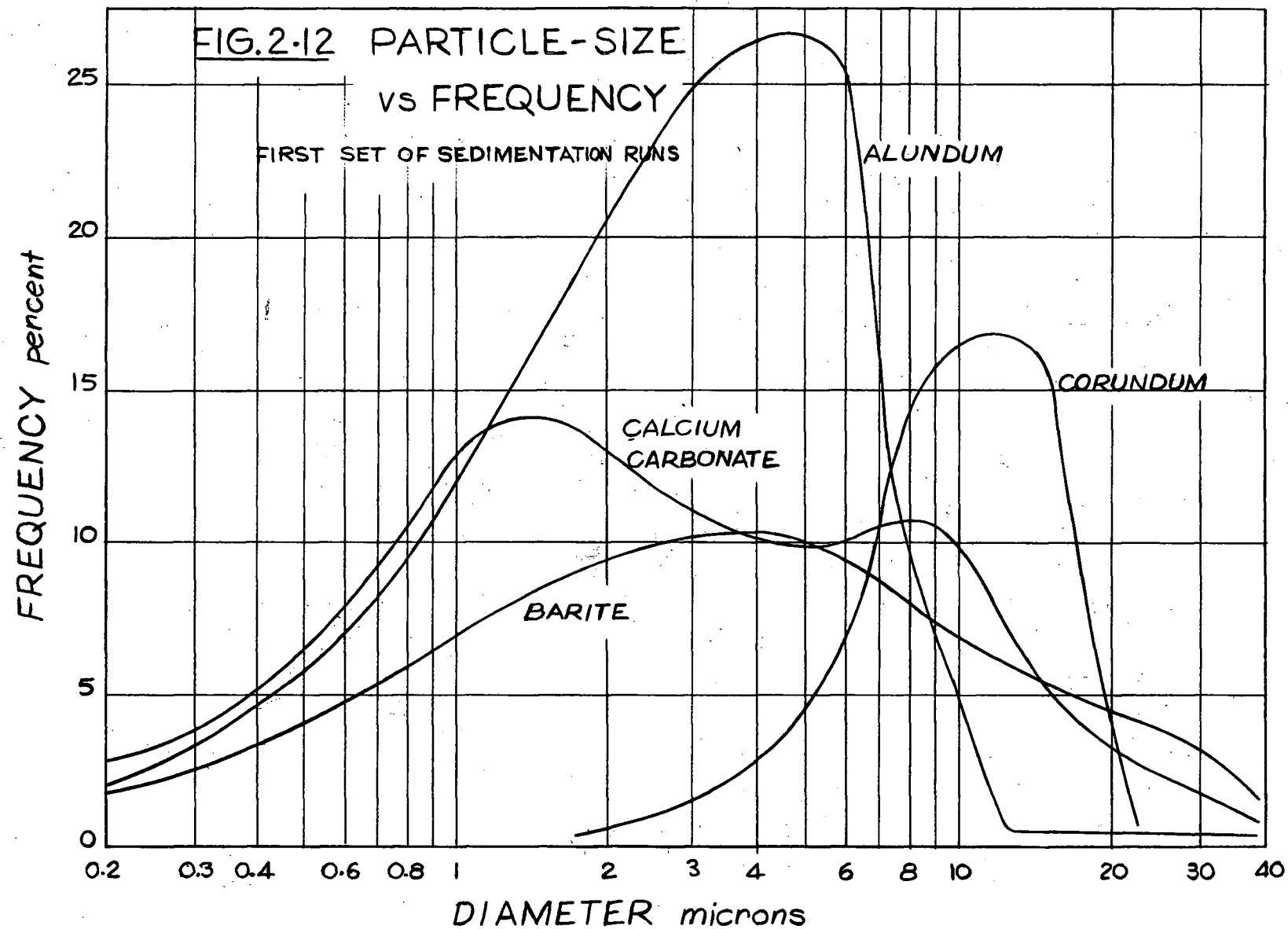
FIG. 2-12 PARTICLE-SIZE vs FREQUENCY
FIRST SET OF SEDIMENTATION RUNS
ALUNDUM
CORUNDUM
CALCIUM CARBONATE
BARITE
FREQUENCY percent
0
5
10
15
20
25
0.2
0.3
0.4
0.6
0.8
1
2
3
4
6
8
10
20
30
40
DIAMETER microns

Table 2.6 below gives the arithmetic mean $\bar{d}$, standard deviation s, geometric mean $\bar{d}_g$ and geometric deviation s_g for all runs as found by the methods explained in Appendix B. The weighted averages for the corresponding runs of each set are shown in brackets. The sample weight in air used for each run is also given.

Table 2.7 on page 40 summarizes all the properties calculated.

TABLE 2.6. DUST SAMPLE MEANS AND DEVIATIONS

	CORUNDUM	BARITE	CALCIUM CARBONATE	ALUNDUM
Arithmetic Mean, $\bar{d}$	12.7	15.1	11.1	8.76
	(12.8)	(14.5)	(10.8)	(8.12)
	12.8	13.8	10.7	7.66
Standard Deviation, s	4.20	11.7	8.77	12.7
	(4.23)	(10.7)	(8.66)	(12.0)
	4.26	9.49	8.57	11.4
Geometric Mean, $\bar{d}_g$	11.9	10.6	7.41	5.07
	(11.9)	(10.5)	(7.11)	(4.84)
	12.0	10.3	6.76	4.67
Geometric Deviation, s_g	1.45	2.63	2.75	2.58
	(1.46)	(2.51)	(2.90)	(2.52)
	1.48	2.37	2.98	2.46
Sample Weight, mg.	700	428	778	521
	654	403	843	717

TABLE 2.7. PARTICLE PROPERTIES

PARTICLE PROPERTY (For description see Appendix)	DUST SAMPLE			
	CORUNDUM	BARITE	CALCIUM CARBONATE	ALUNDUM
Arithmetic Mean, $\bar{d}$	12.8	14.5	10.8	8.12
Standard Deviation, s	4.23	10.7	8.66	12.0
Mode, m	13.5	4.5	1.5	5.0
Asymmetry Parameter, A	-0.17	0.94	1.07	0.26
Median, M	12.8	12.2	8.9	5.0
Upper Quartile,	15.8	21.0	15.7	7.0
Lower Quartile.	9.6	5.9	3.8	3.1
Inter Quartile Range	6.2	15.1	11.9	3.9
The 5%-95% Range	14.0	32.2	28.5	36.3
Skewness Parameter, S	1.03	2.10	2.40	8.55
Coef. of Variation, ϕ	0.331	0.738	0.802	1.48
Geom. Mean, $\bar{d}_g$	11.9	10.5	7.11	4.84
Geom. Deviation, s_g	1.46	2.51	2.90	2.52
Geom. Coef. of Variation, ϕ_g	0.123	0.239	0.408	0.521
Specific Gravity, G	3.85	4.50	2.71	3.58

CHAPTER 3

3.1 EXPERIMENTAL DESIGN

Previous work on a wet type dust collector, similar to the one being tested in this presentation, has shown that the penetration depends on the test dust, the Reynolds number and the collector nozzle geometry. (16). A dimensionless analysis can be set up to yield the relationship

$$\pi = K\,(D)^p \quad (\frac{\rho\, d\, V}{\mu})^q \quad (\frac{a}{\delta})^r$$

$$= K \cdot D^p \,.\, Re^q \cdot J^r \qquad (3.1)$$

where

K = a constant

D = some unknown property which characterizes the dust, and which will be investigated later,

ρ = the density of the air stream at the nozzle throat

μ = the viscosity of the air

V = the nozzle (jet) velocity

δ = the width of the nozzle throat

a = the distance from the nozzle throat to the collector mean water surface.

Another investigator, Semrau (15), has recently stated that the penetration is dependent upon the energy expended in the collector, which of course depends largely upon the velocity of the air stream. Since the present writer has worked with essentially constant values of δ, ρ and μ; the correlation is given in terms of nozzle velocity, V, in thousands of feet per minute, so that the correlating equation becomes

$$\pi = K \cdot D^p \,.\, V^q \,.\, J^r \qquad (3.2)$$

3.1.1 THE FACTORIAL PLAN

The relation of Equation (3.2) can be investigated by either the classical approach or the factorial approach.

The classical plan, often referred to as the ideal experiment, is one in which all variables are held constant except the one under study. This plan is the most commonly used but may not be the best. The factorial plan (7,9) is more efficient because it yields more information for the same amount of effort. It is always more accurate than a classical plan but is restricted to only two types of general experimental functions. Furthermore the class of function must be known beforehand. The first class has the general formula

$$R = f_1(X) + f_2(Y) + \ldots$$

The more usual second class has the form

$$R = f(X) \cdot f(Y) \ldots$$

which can be treated as a special case of the first by taking logarithms, so that the products function becomes

$$\log R = \log f_1(X) + \log f_2(Y) + \ldots$$

Since the function relation, Equation (3.2), is a product type, the factorial approach was used.

The three dependent variables (D, V and J) are arranged in the form of a 4 x 4 Latin square involving 16 runs, one run for each of 16 conditions prescribed by the square. The Latin square is shown in Figure 3.1.

VELOCITY → 1000 fpm	9.02	14.13	6.84	11.81	
Barite	6.85	13.7	20.6	27.4	←'J' Values
Corundum	27.4	6.85	13.7	20.6	
Alundum	20.6	27.4	6.85	13.7	
Calcium Carbonate	13.7	20.6	27.4	6.85	

Figure 3.1 Dust Collector Experimental Plan

The four selected levels of J are systematically placed within the Latin square so that no two of the same J values appear within a column or a row. Next, the four levels of the variable V are randomly assigned to the column headings, and the four test dusts are randomly assigned to the row headings. The 16 runs are made and the Latin square is filled in with the values of the dependent variable, penetration, as shown symbolically below. Since all three factors have four levels, 4^3 or 64 runs would have to be made to obtain the same precision by the classical method as can be obtained from 16 runs using the factorial method (7,9).

In general, the factorial procedure involves taking the log average of the penetrations along each of the 4 levels of D, V and J. The antilogs of the averages are used to determine the function equation.

If the logarithms of the experimental values of penetration are averaged over a single level of D, the effects of those factors that are changing (V and J in this case) will remain the same from one D level to the next. The proof is as follows:

Consider the Latin square shown below where the π's represent the values of penetration corresponding to each set of independent variables - e.g. π_{23} is the value of penetration obtained from a test run using dust D_2 at velocity V_3 and jet condition J_2.

	V_1	V_2	V_3	V_4
D_1	$\pi_{11}^{J_1}$	$\pi_{12}^{J_2}$	$\pi_{13}^{J_3}$	$\pi_{14}^{J_4}$
D_2	$\pi_{21}^{J_4}$	$\pi_{22}^{J_1}$	$\pi_{23}^{J_2}$	$\pi_{24}^{J_3}$
D_3	$\pi_{31}^{J_3}$	$\pi_{32}^{J_4}$	$\pi_{33}^{J_1}$	$\pi_{34}^{J_2}$
D_4	$\pi_{41}^{J_2}$	$\pi_{42}^{J_3}$	$\pi_{43}^{J_4}$	$\pi_{44}^{J_1}$

Re-writing the function relation (Equation 3.2) as

$$\pi = F[D] \cdot F[V] \cdot F[J] \tag{3.3a}$$

and taking logarithms, we have

$$\log \pi = \log F[D] + \log F[V] + \log F[J] \tag{3.3b}$$

Writing the four equations covering the horizontal D_1 row

$$\log \pi_{11} = \log F[D_1] + \log F[V_1] + \log F[J_1]$$

$$\log \pi_{12} = \log F[D_1] + \log F[V_2] + \log F[J_2]$$

$$\log \pi_{13} = \log F[D_1] + \log F[V_3] + \log F[J_3]$$

$$\log \pi_{14} = \log F[D_1] + \log F[V_4] + \log F[J_4]$$

$$\therefore \sum \log \pi_{1j} = 4 \log F[D_1] + \log F\{[V_1] \dots F[V_4]\} + \log\{F[J_1] \dots F[J_4]\} \tag{3.4a}$$

Repeating the same procedure for the D row then

$$\log \pi_{2j} = 4 \log F\left[D_2\right] + \log\left\{F\left[V_1\right]\ldots F\left[V_4\right]\right\} + \log\left\{F\left[J_1\right]\ldots F\left[J_4\right]\right\} \qquad (3.5a)$$

Equation (3.4a) and Equation (3.5a) can be rewritten as

$$\log F\left[D_1\right] = \frac{\sum \log \pi_{1j}}{4} - \log k \qquad (3.4b)$$

$$\log F\left[D_2\right] = \frac{\sum \log \pi_{2j}}{4} - \log k \qquad (3.5b)$$

and so on for the D_3 and D_4 levels. Thus all changes in the log average of the result are wholly due to the effect of the dust alone. Similar results can be shown when the logarithmic average is taken over the four V levels, and over the four J levels.

The logarithms of the penetrations then are summed along each row, along each column, and diagonally as well to cover the 4 J levels.

Each of the 12 sums obtained is then averaged and the antilog is taken. The 12 values of the log average penetrations can be represented by the following equations where each π is the antilog of a log average.

Rows	Columns	Diagonals
$\pi_{D_1} = k\ F\left[D_1\right]$;	$\pi_{V_1} = k'\ F\left[V_1\right]$;	$\pi_{J_1} = k''\ F\left[J_1\right]$
$\pi_{D_2} = k\ F\left[D_2\right]$;	$\pi_{V_2} = k'\ F\left[V_2\right]$;	$\pi_{J_2} = k''\ F\left[J_2\right]$
$\pi_{D_3} = k\ F\left[D_3\right]$;	$\pi_{V_3} = k'\ F\left[V_3\right]$;	$\pi_{J_3} = k''\ F\left[J_3\right]$
$\pi_{D_4} = k\ F\left[D_4\right]$;	$\pi_{V_4} = k'\ F\left[V_4\right]$;	$\pi_{J_4} = k''\ F\left[J_4\right]$

For each D level, i.e. for each test dust, there is a log average value of penetration, π_D. Similarly, for each V level there is a π_V and for each J level there is a π_J.

Next, curves are drawn for π_D versus D, π_V versus V, and π_J versus J. Such curves yield the following equations.

$$\pi_D = k \; F \; [D] \tag{3.6}$$

$$\pi_V = k' \; F \; [V] \tag{3.7}$$

$$\pi_J = k'' \; F \; [J] \tag{3.8}$$

Solving these three equations for F [D], F [V] and F [J] and substituting into Equation (3.3a) we obtain

$$\pi = K \; \pi_D \cdot \; \pi_V \; \cdot \pi_J \tag{3.9}$$

where $K = \frac{1}{kk'k''}$ and is evaluated from the data.

Equation (3.9) is the relationship which will determine π for all of the 64 combinations of D, V and J even though only 16 runs were made.

The function relation Equation (3.2) would yield the same values of π as Equation (3.9) provided the 3 correlation equations , Equations (3.6), (3.7) and (3.8) are perfect. This is highly unlikely, but in any event, Equation (3.2) may fit similar data with other test dusts which could not be done using Equation (3.9).

3.1.2 ANALYSIS OF VARIANCE

Before processing the data in the Latin square to yield regression equations, it is possible to apply the analysis of variance test.

Such an analysis is valuable in determining the extent to which the various factors influence the penetration and also to determine the relative magnitude of the error. An estimate of the variance between rows, columns, diagonals, and residual or error can be made by comparing the variance due to residual or error with the three factor variances so that the significance of each of the three factors on penetration is determined. Should a perfect functional relationship exist, the residual variance will be zero.

The analysis of variance test is performed on the data in Section 4.1.1. The theory involved in such an analysis (5,6) is so involved and lengthy that it is omitted from this presentation.

CHAPTER 4

4.1 ANALYSIS OF DATA

Table 4.1 shows the values of penetration obtained for two experiments as well as the mean of the two which is given in brackets. The average amount of sample test dust used is given under each test dust.

The value of J used for each run is shown in the upper right corner of the blocks.

TABLE 4.1 DUST COLLECTOR PENETRATION RESULTS

Penetration, %

Velocity (1000fpm) →	9.02	14.13	6.84	11.81
Barite 5 gm.	6.85 1.05 (1.05) 1.05	13.7 0.575 (0.685) 0.795	20.6 1.75 (1.87) 1.98	27.4 1.16 (1.19) 1.21
Corundum 10 gm.	27.4 0.130 (0.157) 0.183	6.85 0.114 (0.138) 0.161	13.7 0.171 (0.186) 0.201	20.6 0.089 (0.121) 0.153
Alundum 1 gm.	20.6 8.70 (8.68) 8.65	27.4 5.20 (5.27) 5.34	6.85 7.96 (7.93) 7.90	13.7 5.09 (5.12) 5.15
Calcium Carbonate 1.5 gm.	13.7 4.17 (4.21) 4.24	20.6 2.66 (2.77) 2.88	27.4 6.57 (6.79) 7.00	6.85 2.54 (2.72) 2.89

4.1.1 ANALYSIS OF VARIANCE TABLE

The steps involved in determining an analysis of variance table are listed below, and are followed immediately by an example calculation using the data of Table 4.1.

Suppose we make a null hypothesis that all four test dusts give approximately the same penetration, and moreover that it does not matter what velocity or water level is used in determining π . Under such an hypothesis the four independent estimates of variance namely D, V, J and residual or error are all estimates of the variance of a common parent population where variability exists for reasons other than D, V, and J.

When a sum of squares is divided by the corresponding number of degrees of freedom on which the sum of squares is based, we are estimating a variance. Snedecor's Variance Ratio Test (5,6) may be used to test the mutual compatibility of variance estimates.

1. Sum all the values of $\log \pi$ in each row to get the row totals. Square each row total, divide it by the number of items in the row (in this case four), and add the results. (The same result is obtained in the following example by summing the squares of the row totals and then dividing by four).
2. Repeat this process for the columns and diagonals.
3. Find the sum of the squares of all the sixteen values in the Latin square - i.e. $\sum(\log \pi)^2$.
4. Find the square of the sum of the above values - i.e. $(\sum \log \pi)^2$.
5. Obtain the "Correction Factor" by dividing the result in item (4) by the total number of values - i.e. 16 in this case.

6. Subtract the Correction Factor from the results of items (1), (2) and (3). This process yields the values 6.401, 0.198, 0.026 and 6.661 which are listed in Table 4.2 under the heading "Sum of Squares".
7. Find the "Sum of the Squares" of the Residual by difference to obtain the value 0.036.
8. Find the number of degrees of freedom in each row of Table 4.2 by subtracting unity from the number of rows. Repeat for the columns and the diagonals. The total degrees of freedom is found by subtracting unity from the total number of values in the Latin square. Find the residual degrees of freedom by difference.
9. Find the variance estimate by dividing the Sum of Squares by the degrees of freedom.

The notation is as follows:

1. Rows refer to the four dusts, i.e. four levels of D.
2. Columns refer to the four levels of V.
3. Diagonals refer to the four levels of J.
4. Residuals refer to unaccounted for variables and error.

Because the analysis of variance test is applicable only to functions of the summation type, the logs of penetration must be used in the analysis.

	Log Penetration				Row Totals	Row Totals Squared
	0.0212	-0.1643	0.2718	0.0755	0.2042	0.042
	-0.8041	-0.8601	-0.7305	-0.9172	-3.3119	10.98
	0.9385	0.7218	0.8993	0.7093	3.2689	10.69
	0.6243	0.4425	0.8319	0.4346	2.3333	5.45
Column Totals	0.7799	0.1399	1.2725	0.3022	2.4945	27.16
Column Totals Squared	0.608	0.020	1.630	0.091		2.349
Diagonal Totals	0.4950	0.4388	0.7356	0.8251		
Diagonal Totals Squared	0.245	0.193	0.541	0.681		1.660

Total Sum of Squares of Items = $\sum (\log \pi)^2$ = 7.050

Correction Factor = $\frac{(\text{Sum of } \log \pi)^2}{\text{Number of Items}} = \frac{(2.4945)^2}{16}$ = 0.389

The sum of squares for each source of variance was determined and an analysis of variance table made as shown in ~~Figure~~ Table 4.2.

TABLE 4.2 ANALYSIS OF VARIANCE TABLE

Source of Variance	Sum of Squares	Degrees of Freedom	Variance Estimate	F Ratio
Between Rows (Dust)	6.401	3	2.13	355
Between Columns (Velocity)	0.198	3	0.066	11
Between Diagonals (Water Level)	0.026	3	0.0087	1.4
Residual	0.036	6	0.006	
Total	6.661	15		

Comparing the variance estimates of the three factors with the residual variance we can conclude that

(a) An hypothesis that the row means are equal can certainly be rejected.

(b) Variation due to column means, although not as great as that due to row means, is significant.

(c) Variation due to diagonals (water level) is not too far different from that due to error (residual) and the null hypothesis that the diagonal means are equal could not be rejected. These conclusions can be confirmed by applying the F-test at the 95 percent significant level.

The analysis of variance does not give the regression equation.

4.1.2 FACTORIAL PLAN RESULTS

The factorial plan was applied to the data of Table 4.1 as shown below.

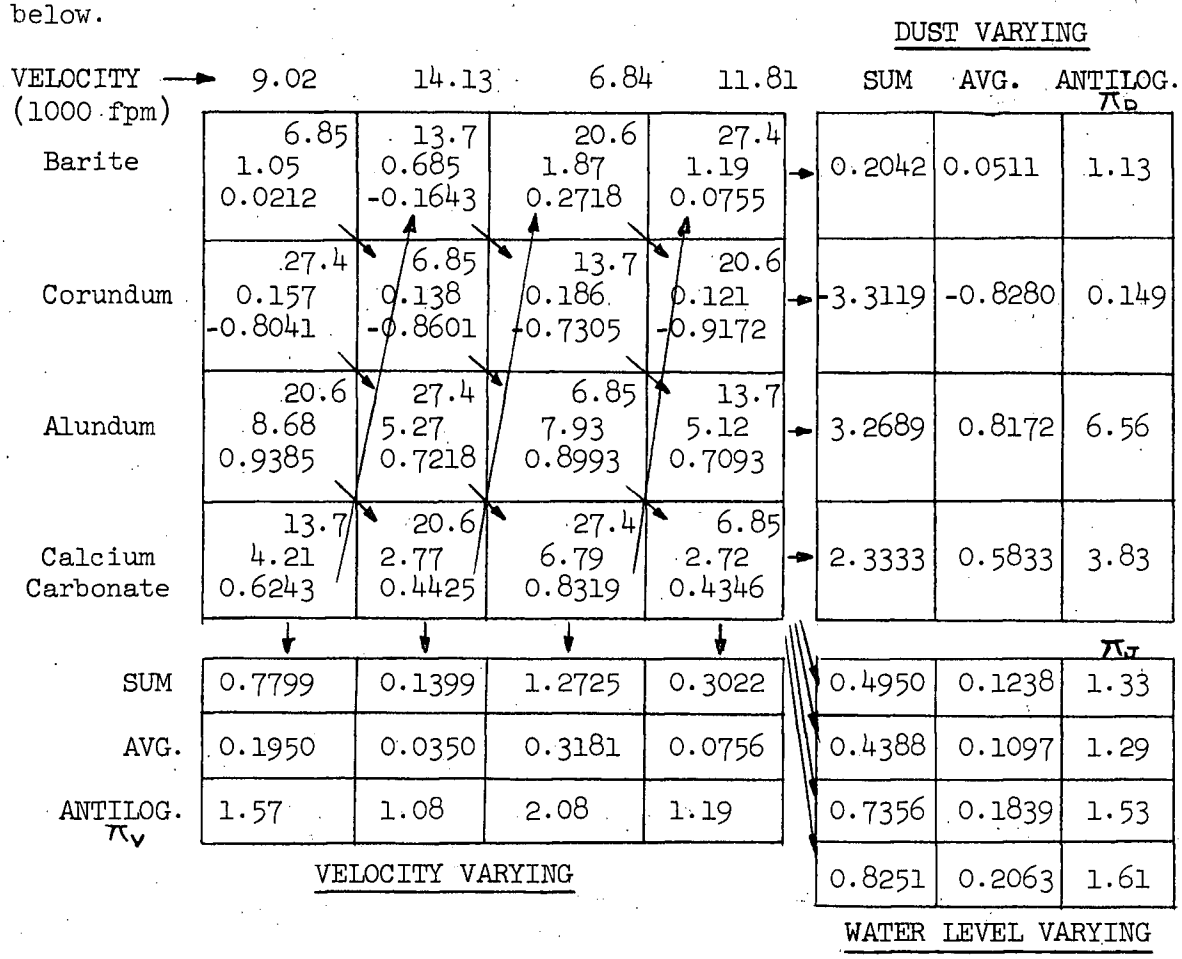

TABLE 4.3 FACTORIAL PLAN RESULTS

DUST, D	π_D	VELOCITY, V (1000fpm)	π_V	NOZZLE GEOMETRY, J	π_J
Barite	1.13	6.84	2.08	6.85	1.33
Corundum	0.149	9.02	1.57	13.7	1.29
Alundum	6.56	11.81	1.19	20.6	1.53
Calcium Carbonite	3.83	14.13	1.08	27.4	1.61

Table 4.3 gives a summary of the results of the factorial plan.

The constant K in Equation (3.9), $\pi = K(\pi_D \cdot \pi_V \cdot \pi_J)$ can be computed from the experimental values of π in the Latin square and from the corresponding values of π_D, π_V and π_J.

As an example, the value of K for the observation using barite at a velocity of 6840 fpm and J = 20.6 is

$$K = \frac{\pi}{\pi_D \cdot \pi_V \cdot \pi_J}$$

$$= \frac{1.87}{1.13\ (2.08)(1.53)} = 0.520$$

This K value can be checked by repeating the calculation on any other data point in the Latin square.

The following square shows the K value computed for each of the 16 runs. The differences in K's indicate how badly the data deviate.

0.445	0.435	0.520	0.550
0.417	0.645	0.465	0.446
0.550	0.462	0.436	0.508
0.543	0.438	0.529	0.449

The mean K is 0.49 with a standard deviation of 0.06, or about 12%.

Equation (3.9) can now be written as

$$\pi = 0.49\ \pi_D \cdot \pi_V \cdot \pi_J \qquad (4.1)$$

Equation (4.1) as it stands, can be used to determine the penetrations for all 64 combinations of π_D, π_V and π_J even though only 16 runs were made.

Example:

The penetration for Alundum at a velocity of 14,130 fpm and J equal to 6.85 is

$$\pi = 0.49 \left(\pi_D \right) \left(\pi_V \right) \left(\pi_J \right)$$

$$= 0.49 \ (6.56) \ (1.08) \ (1.33)$$

$$= 4.62 \text{ with an uncertainty of about } \pm 12\%.$$

The data given in Table 4.3 can be used only in conjunction with Equation 4.1 since the component penetrations, π_D's, π_V's, π_J's represent log averages rather than discrete values. By plotting π_J versus J, π_V versus V and π_D versus some suitable parameter describing the test dust, best fit equations can be determined.

The geometric coefficient of variation, $\phi_g = \frac{s_g}{\bar{d}_g}$, was chosen to describe the test dust, for reasons which are stated in the discussion of results, Section 4.3.

Least squares methods were used to derive the correlation equations. They are shown plotted in Figures 4.1 and 4.2. The equations found are given below

$$\pi_D = 39.4 \ \phi_g^{2.61} \qquad (4.2)$$

$$\pi_V = 12.5 \ V^{-0.939} \qquad (4.3)$$

$$\pi_J = 0.934 \ J^{0.146} \qquad (4.4)$$

Substituting for π_D, π_V and π_J into Equation (4.1)

$$\pi = 0.49 \ \pi_D \cdot \pi_V \cdot \pi_J \qquad (4.1)$$

we obtain

$$= 233 \ \phi_g^{2.61} \ V^{-0.939} \ J^{0.146} \qquad (4.5)$$

which is the required function relation whose general form was given by Equation (3.1).

A somewhat less accurate relation was obtained by replacing the term $39.4\ \phi_g^{2.61}$ in Equation (4.5) by the term $3.2\ \phi^{2.60}$. See Figure 4.1.

A more accurate correlation equation, although more cumbersome to use, was obtained by fitting second-order equations to the curves π_D versus ϕ_g and π_V versus V.

These plots are given in Figures 4.3 and 4.4.

The correlation equation in this case becomes

$$\pi = 0.49 \left(\pi_D \cdot \pi_V \cdot \pi_J \right)$$

$$= 0.49 \left\{ 25(\phi_g^2 - 0.0111)\ 0.0125\ (V^2 - 31.5V + 330)\ 0.934\ J^{0.146} \right\}$$

and

$$= 0.148\ (\phi_g^2 - 0.0111)(V^2 - 31.5V + 330)J^{0.146} \quad (4.6)$$

for V in thousands of feet per minute.

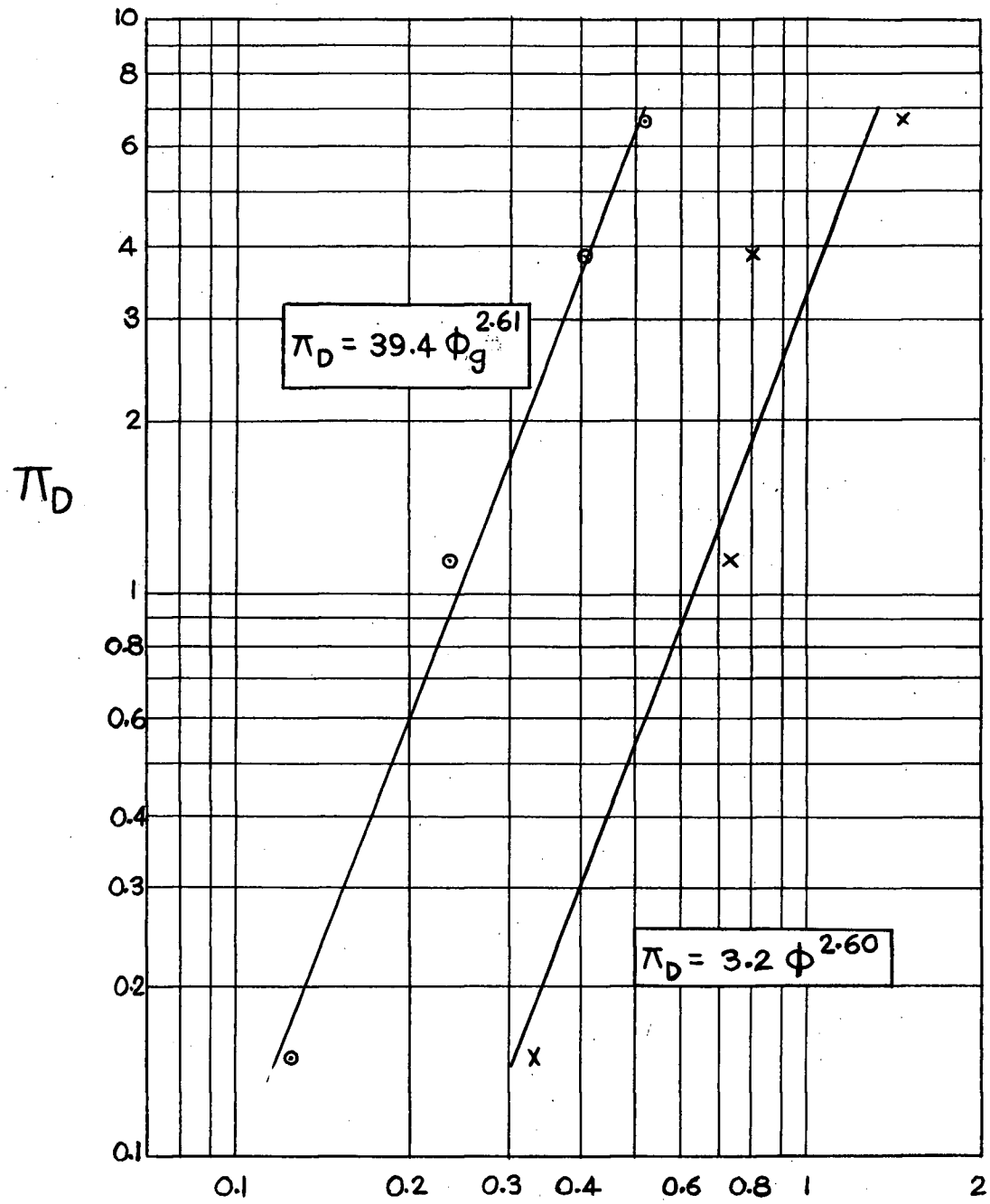

FIG.4-1 CORRELATION OF π_D WITH ϕ_g AND ϕ

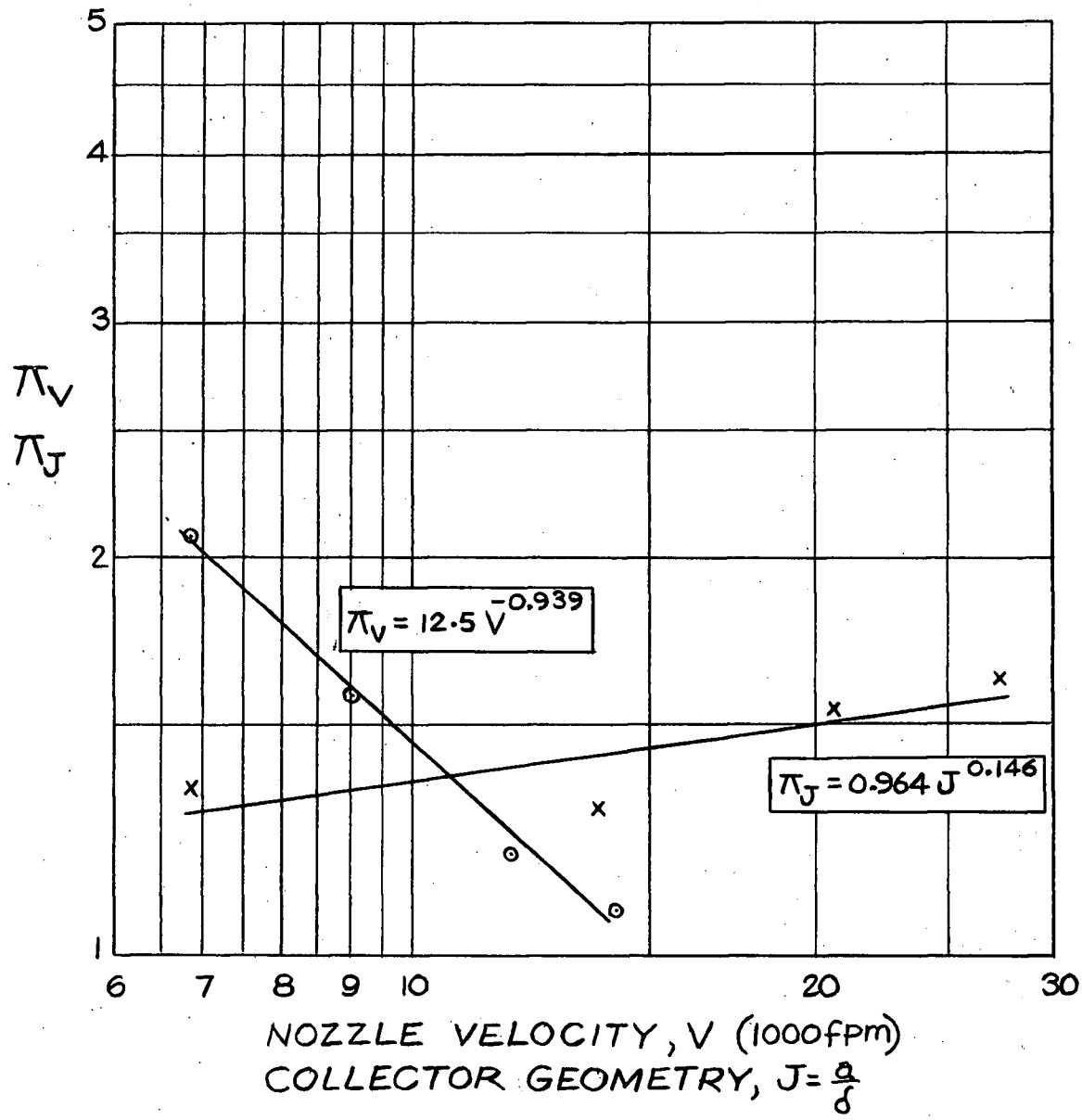

FIG. 4.2 CORRELATION OF π_V WITH V AND π_J WITH J

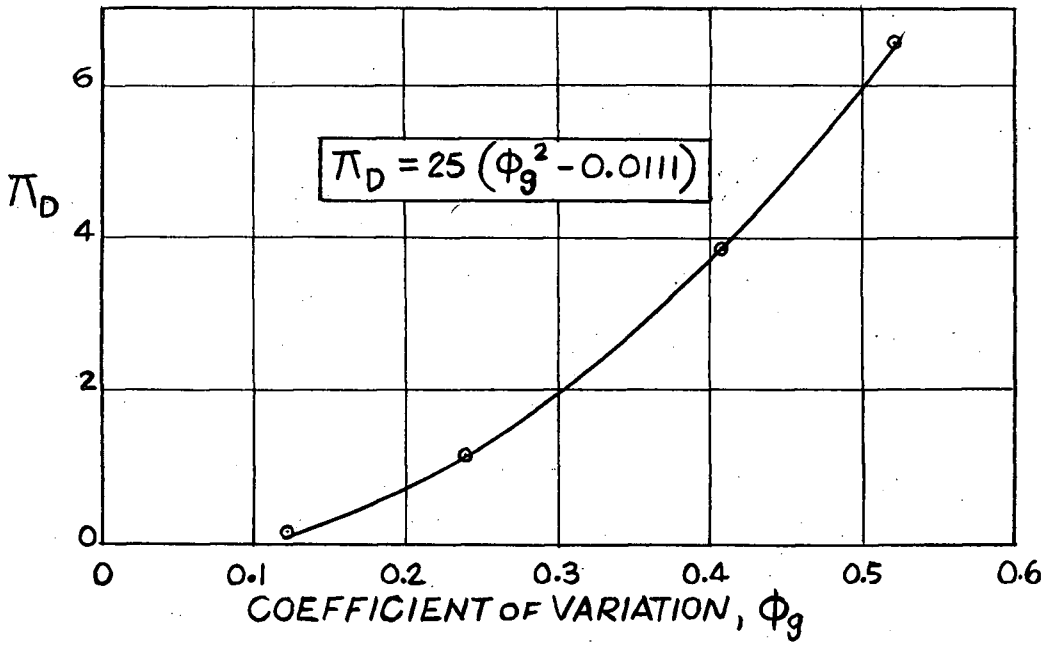

FIG. 4·3 CORRELATION OF π_D WITH ϕ_g

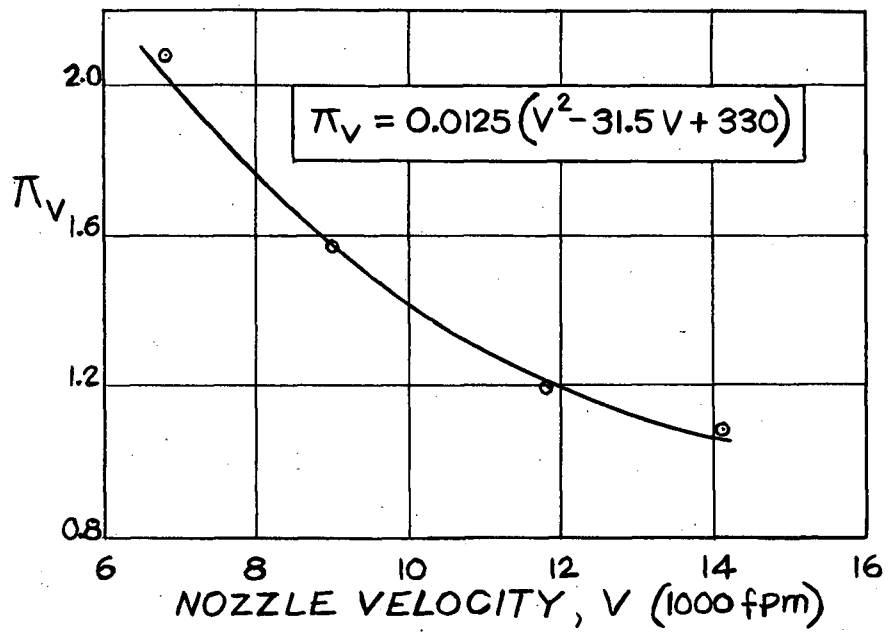

FIG. 4·4 CORRELATION OF π_V WITH V

A summary of the results of the factorial experiment and the derived equation is given below.

TABLE 4.4 SUMMARY OF RESULTS

Dust	ϕ_g	π_D	V	π_V	J	π_J
Barite	0.239	1.13	6.84	2.08	6.85	1.33
Corundum	0.123	0.149	9.02	1.57	13.7	1.29
Alundum	0.521	6.56	11.81	1.19	20.6	1.53
Calcium Carbonate	0.408	3.83	14.13	1.08	27.4	1.61

$$\pi = 0.49 \quad \pi_D \cdot \pi_V \cdot \pi_J \tag{4.1}$$

$$\pi_D = 39.4 \ \phi_g^{2.61} \tag{4.2}$$

$$\pi_V = 12.5 \ V^{-0.939} \tag{4.3}$$

$$\pi_J = 0.964 \ J^{0.146} \tag{4.4}$$

$$\pi = 233 \ \phi_g^{2.61} \ V^{-0.939} \ J^{0.146} \tag{4.5}$$

Note: Values of π_D, π_V, π_J shown in the table and Equations (4.2), (4.3) and (4.4) are to be used only in Equation (4.1) and are not to be used alone.

Equation (4.5) was plotted as π versus V with J = 13.7 for each of the four test dusts. These curves are shown in Figure 4.5. Equation (4.5) was also plotted as π versus ϕ_g with J = 13.7 for velocities of 7,000 fpm and 14,000 fpm. These curves are shown in Figure 4.6.

Equation (4.1) was then plotted on the same graphs for comparison.

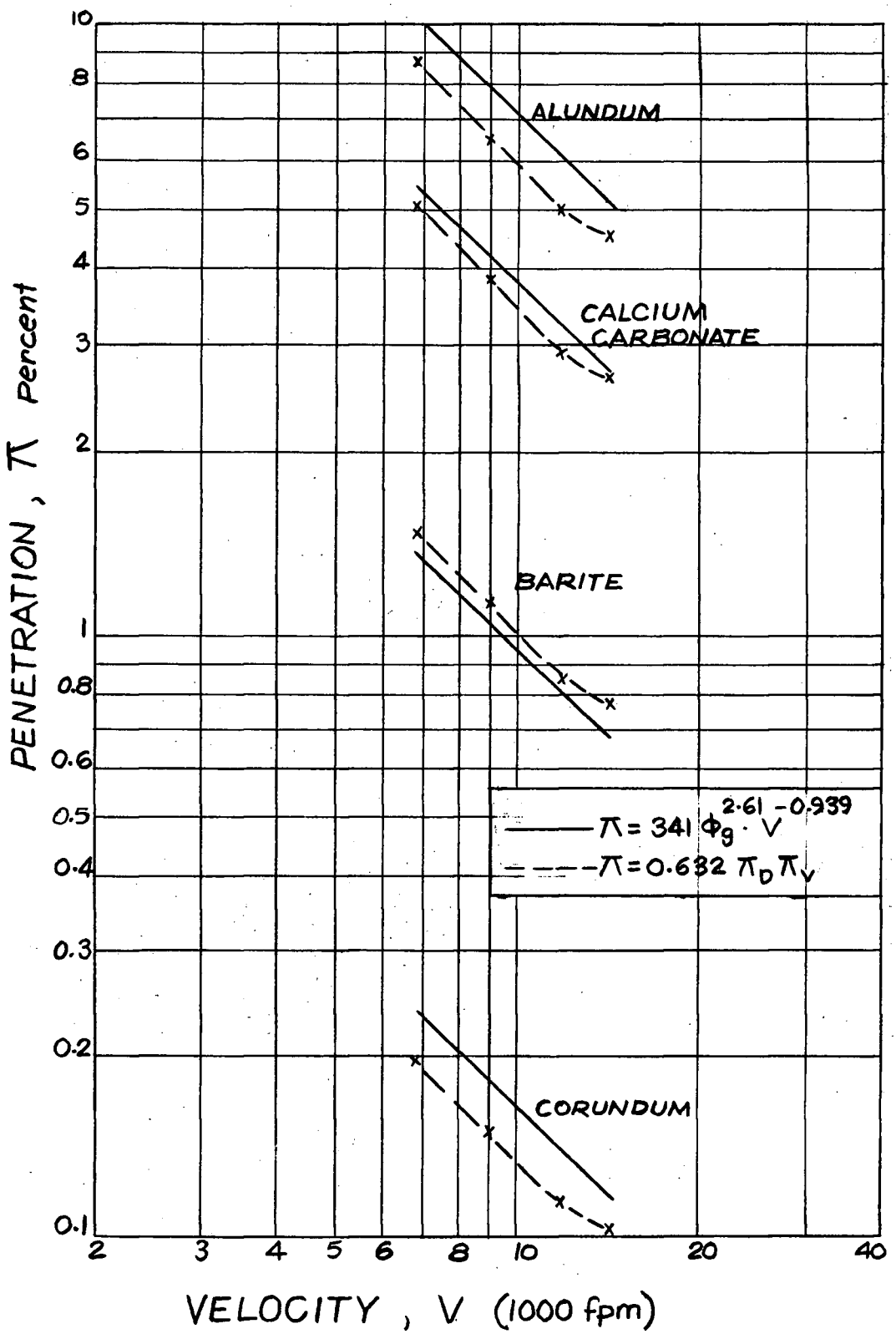

FIG. 4·5 PENETRATION vs VELOCITY FOR J = 13.7

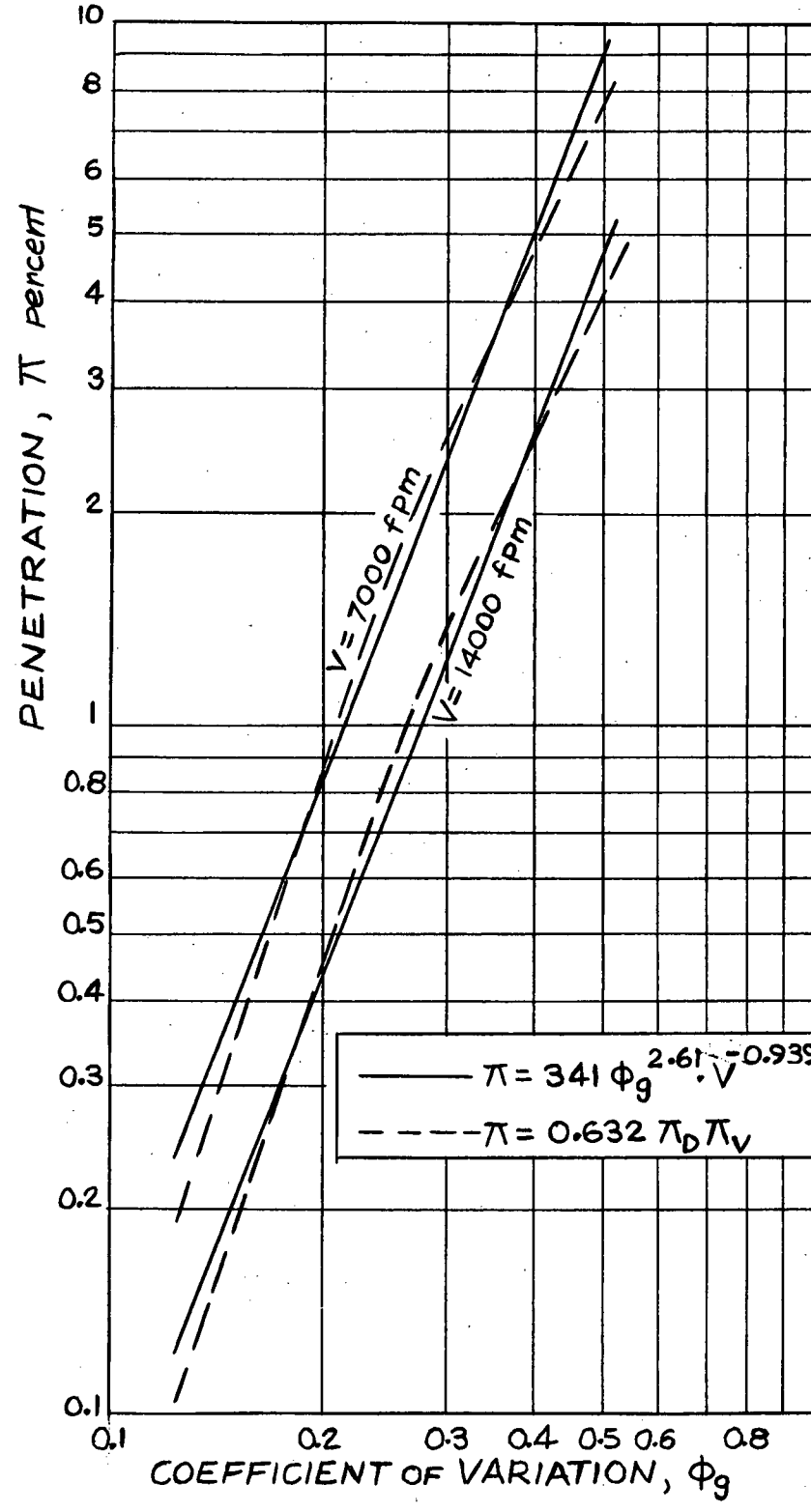

FIG. 4.6 PENETRATION vs ϕ_g FOR J=13.7

For J = 13.7, Equations (4.5) and (4.1) take the forms

$$\pi = 341\ \phi_g^{2.61}\ V^{-0.939} \qquad (4.7)$$

and

$$\pi = 0.632\ \pi_D \cdot \pi_V \qquad (4.8)$$

Instead of assuming π_D to be a function of ϕ_g only, Equation (4.2), perhaps a better relationship is given by Equation (4.9a) below.

$$\pi_D = K.\ \phi_g^{\ell}.\ S^m\ .\ G^n \qquad (4.9a)$$

where K is a constant

and ϕ_g = geometric coefficient of variation

S = skewness parameter

$$= \frac{\text{upper 45 \% range}}{\text{lower 45 \% range}} \quad \text{(See Appendix B)}$$

G = specific gravity of test dust with respect to water.

The constant K and the exponents ℓ, m, n are determined by setting Equation (4.9a) equal to the corresponding values of π_D for the four dusts, i.e.

for Barite $\quad K\ (0.239)^{\ell}\ .(2.10)^m\ (4.50)^n = 1.13$

for Corundum $\quad K\ (0.123)^{\ell}\ .(1.03)^m\ (3.85)^n = 0.149$

for Alundum $\quad K\ (0.521)^{\ell}\ .(8.55)^m\ (3.58)^n = 6.56$

for Calcium Carbonate $\quad K\ (0.408)^{\ell}\ .(2.40)^m\ (2.71)^n = 3.83$

The values of ϕ_g, S, G are given in Table 2.7 for the four dusts.

The four equations are solved for the four unknowns K, ℓ, m, n and Equation (4.9a) becomes

$$\pi_D = 40.1\ \left[\phi_g^{3.26}\ S^{-0.41}\ G^{0.928}\right] \qquad (4.9b)$$

Equations (4.3), (4.4) and (4.9b) are substituted into Equation (4.1) so that

$$\pi = 237\ (\phi_g^{3.26}\ S^{-0.41}\ G^{0.928})\ V^{-0.939}\ J^{0.146} \qquad (4.10)$$

Equation (4.9b) will yield exact values of π_D , of course, for the four dusts tested. The variables ϕ_g , S and G were chosen since it was felt that these three variables contribute more to characterization of the dust than any of the other dust variables.

4.2 THE COMPOUND ERROR

The compound error (7,9) in penetration due to errors in the components of the function relation,

$$\pi = 233\ \phi_g^{2.61}\ V^{-0.939}\ .\ J^{0.146} \qquad (4.5)$$

can be estimated by the relation,

$$\sigma = \left\{ \left[\frac{\partial \pi}{\partial \phi_g} \sigma_\phi \right]^2 + \left[\frac{\partial \pi}{\partial V} \sigma_V \right]^2 + \left[\frac{\partial \pi}{\partial J} \sigma_J \right]^2 \right\}^{\frac{1}{2}}$$

where σ = the compound error in penetration

and $\sigma_\phi, \sigma_V, \sigma_J$ are the errors in estimating ϕ, V and J respectively.

Performing the indicated operations to Equation (4.5), then dividing the result by Equation (4.5), the fractional error obtained is

$$\frac{\sigma}{\pi} = \left\{ \frac{6.82}{\phi_g^2}\sigma_\phi^2 + \frac{0.885}{V^2}\sigma_V^2 + \frac{0.0212}{J^2}\sigma_J^2 \right\}^{\frac{1}{2}} \qquad (4.11)$$

The fractional estimating errors $\frac{\sigma_\phi}{\phi_g}$, $\frac{\sigma_V}{V}$ and $\frac{\sigma_J}{J}$ are calculated as follows:

(1) $\frac{\sigma_J}{J}$: Assuming the water level in the collector can be measured to the nearest 0.1 inch, then $\frac{\sigma^2_J}{J^2}$ is a maximum of 0.0256 for J=6.85 and a minimum of 0.001 for J=27.4.

(2) $\frac{\sigma_V}{V}$: The fractional error in velocity as determined by the equation $V = 1054 \frac{\sqrt{\gamma_1 h_w}}{\gamma_n}$ fpm. is obtained from $\frac{\sigma_V^2}{V^2} = \frac{\sigma_h^2}{4h^2}$ where σ^2_h is the estimating variance in the orifice drop, h_w. Assuming the orifice manometer drop to be in error by 0.2 inch, and the errors in γ_1 and γ_n to be negligible, then $\frac{\sigma_V^2}{V^2}$ is 0.0051 for h = 2.8 which corresponds to a velocity of 6840 fpm. For h = 8.1, which corresponds to a velocity of 14,130 fpm, $\frac{\sigma_V^2}{V^2}$ is 0.00061.

(3) $\frac{\sigma\phi}{\phi_g}$: The fractional error $\frac{\sigma\phi}{\phi_g}$ can be obtained from an estimate of the error in the equivalent spherical diameter which was determined by sedimentation, and is given by,

$$d = 175\sqrt{\frac{\mu}{\rho_p - \rho_f} \cdot \frac{h}{t}} \qquad (2.4)$$

If the estimating errors in μ and h are known, then following the same procedure as before, the fractional error in Equation (2.4) is

$$\frac{\sigma}{d} = \left[\left(\frac{\partial d}{\partial \mu}\right)^2 \sigma_\mu^2 + \left(\frac{\partial d}{\partial h}\right)^2 \sigma_h^2\right]^{\frac{1}{2}}$$

$$= \left[\frac{1}{4\mu^2}\sigma_\mu^2 + \frac{1}{4h^2}\sigma_h^2\right]^{\frac{1}{2}}$$

Assuming h = 20 $\pm$ 0.2 cm. and μ = 0.958 $\pm$ 0.023 centipoise for $\pm$ 1°C., then the terms $\frac{\sigma_h^2}{4h^2}$ and $\frac{\sigma_\mu^2}{4\mu^2}$ in Equation (4.12) become 0.000025 and 0.000144 respectively, so that $\frac{\sigma}{d}$ = 1.3 %. The fraction estimating error in ϕ_g is given by

$$\frac{\sigma_\Phi}{\Phi_g} = \left[\frac{\sigma_s^2}{s_g} + \frac{\sigma_d^2}{\bar{d}_g^2}\right] \quad \text{since } \phi_g = \frac{s_g}{\bar{d}_g}$$

Putting $\frac{\sigma_s}{s_g}$ and $\frac{\sigma_d}{\bar{d}_g}$ both equal to 0.013, then $\frac{\sigma^2\phi}{\phi_g^2} = (0.013)^2 + (0.013)^2 = 0.000338$

The estimating errors $\frac{\sigma\phi}{\phi_g}$, $\frac{\sigma_V}{V}$ and $\frac{\sigma_J}{J}$ can now be substituted into the error Equation, (4.11) to determine maximum and minimum compound errors for Equation (4.5).

$$\left(\frac{\sigma}{\pi}\right)_{max.} = \left[(6.82)0.000338 + (0.885)0.0051 + (0.0212)0.0256\right]^{\frac{1}{2}}$$

$$= \left[(0.0023 + 0.0045 + 0.0005)\right]^{\frac{1}{2}}$$

$$= 8.5\ \%\ \text{at maximum values of V and J.}$$

$$\left(\frac{\sigma}{\pi}\right)_{min.} = \left[0.0023 + (0.885)0.00061 + (0.0212)0.001\right]^{\frac{1}{2}}$$

$$= \left[(0.00230 + 0.00054 + 0.00002)\right]^{\frac{1}{2}}$$

$$= 5.3\ \%\ \text{at maximum values of V and J.}$$

In summary there will be a maximum error of 8.5 % in the regression equation, $\pi = 233\ \phi_g^{2.61}\ V^{-0.939}\ .\ J^{0.146}$ under the following conditions:

(i) the sedimentation room temperature is controlled to $\pm$ 1°C.,

(ii) the height of the sedimentation medium is in error by 0.2 cm. or 1 %,

(iii) the orifice manometer drop is accurate to within 0.2" w.c.,

(iv) the collector water level is accurate to within 0.1 inches.

The error equation can serve as a guide for estimating the component errors should further experimentation be done with this equipment. The maximum error of 8.5 % is below the uncertainty figure of $\pm$ 12 % given in section 4.1.2. This would imply that the four conditions listed above are optimistic or other sources of error are present, such as human error, error due to random sampling of the test dusts and also the neglect of minor variables.

4.3 DISCUSSION OF RESULTS

4.3.1 Goodness of Fit

The function relation, Equation (4.5) shows that ϕ_g plays the most important role of the three independent variables in determining the magnitude of the penetration. This fact, of course, also showed up in the analysis of variance test which indicated there being no doubt the row variance was due to the dust used and not experimental error.

Figures 4.5 and 4.6 indicate how well Equation (4.5) fits the results of the factorial experiment which were given in terms of average penetration namely, π_D , π_V and π_J. Figures 4.5 and 4.6 were drawn for a J value of 13.7. Similar curves could be drawn for the other three levels of J used in the experiment. A point which must be made concerning curves obtained from Equation (4.5) is that they must necessarily all have the same slope. This is due to the type of correlation assumed and would only be otherwise if one or more of the influencing variables were used as a power to which V, ϕ_g or J could be raised.

Researchers in the field (15,16) have obtained unique equations of π versus V for each type of dust tested and the curves do show different slopes. No one has yet determined a correlation of the form $\pi = aV^b$ where 'a' and 'b' contain the variables particle size, distribution, and perhaps particle density. Semrau (15) does mention the fact that 'a' and 'b' are functions of the particle size and the size distribution. However his dusts were not sized.

4.3.2 COEFFICIENT OF VARIATION

The fact that penetration increases with increasing values of ϕ_g has been confirmed using data previously taken by Wighton (16). He determined size distributions for a number of test dusts by microscopy and presented the data in the form of log probability plots. Values of ϕ_g and S obtained from these plots are tabulated below. Opposite these are values of penetration obtained by Wighton using a wet collector with a different nozzle geometry but otherwise similar to the collector used in the present work.

SAMPLE	G	ϕ_g approx	S approx	π
Silica	2.65	0.1	1.4	0.4
Limestone	2.81	0.1	0.8	0.5
Silica		0.15	1.5	0.8
Limestone		0.2	1.2	2.1
A.C. Fine	2.68	0.2	0.8	2.5
Silica		0.25	1.4	1.8
Alundum	3.58	0.3	2.1	5.3
Limestone		0.3	1.5	6.0
A.C. Fine		0.35	2.1	4.6

This correlation of π with ϕ_g occurs despite a different sizing technique, a different nozzle geometry, and a different method for computing ϕ_g. In this table, ϕ_g was approximated by assuming a log-normal distribution, computing $s_g = \frac{84.13\% \text{ size}}{50\% \text{ size}}$ and dividing by the

value of $\bar{d}_g$ obtained from the 50% size. Since none of the curves from which ϕ_g was calculated were log-normal, the value of ϕ_g is in error. In fact, values of ϕ_g determined graphically for the dust samples used in this presentation are all below the calculated values given in Table 2.7, some by as much as 65 percent.

Figure 4.7 shows some theoretical log-normal distribution functions which plot as straight lines on log-probability paper.

For log-normal plots ϕ_g is given as

$$\phi_g = \frac{84.13\% \text{ size}}{(50\% \text{ size})^2} \qquad \text{(Appendix B)}$$

and can be found by inspection of the curves of Figure 4.7. The curves are labelled with their unique values of ϕ_g . Note that although a curve can have only one value of ϕ_g , a given value of ϕ_g may apply to more than one curve.

Recalling the finding that penetration increases with ϕ_g , it is possible to explain why this should be so.

The coefficient of variation $\phi_g = \frac{s_g}{\bar{d}_g}$ will increase provided that

1) $\bar{d}_g$ decreases for a constant s_g .

2) s_g increases for a constant $\bar{d}_g$.

3) s_g and $\bar{d}_g$ change in favorable directions.

The three parallel curves of Figure 4.7 illustrate three different distributions having different geometric means but identical geometric deviations. The coefficient of variation is shown to increase in this case as $\bar{d}_g$ decreases. Other conditions remaining equal, we would expect

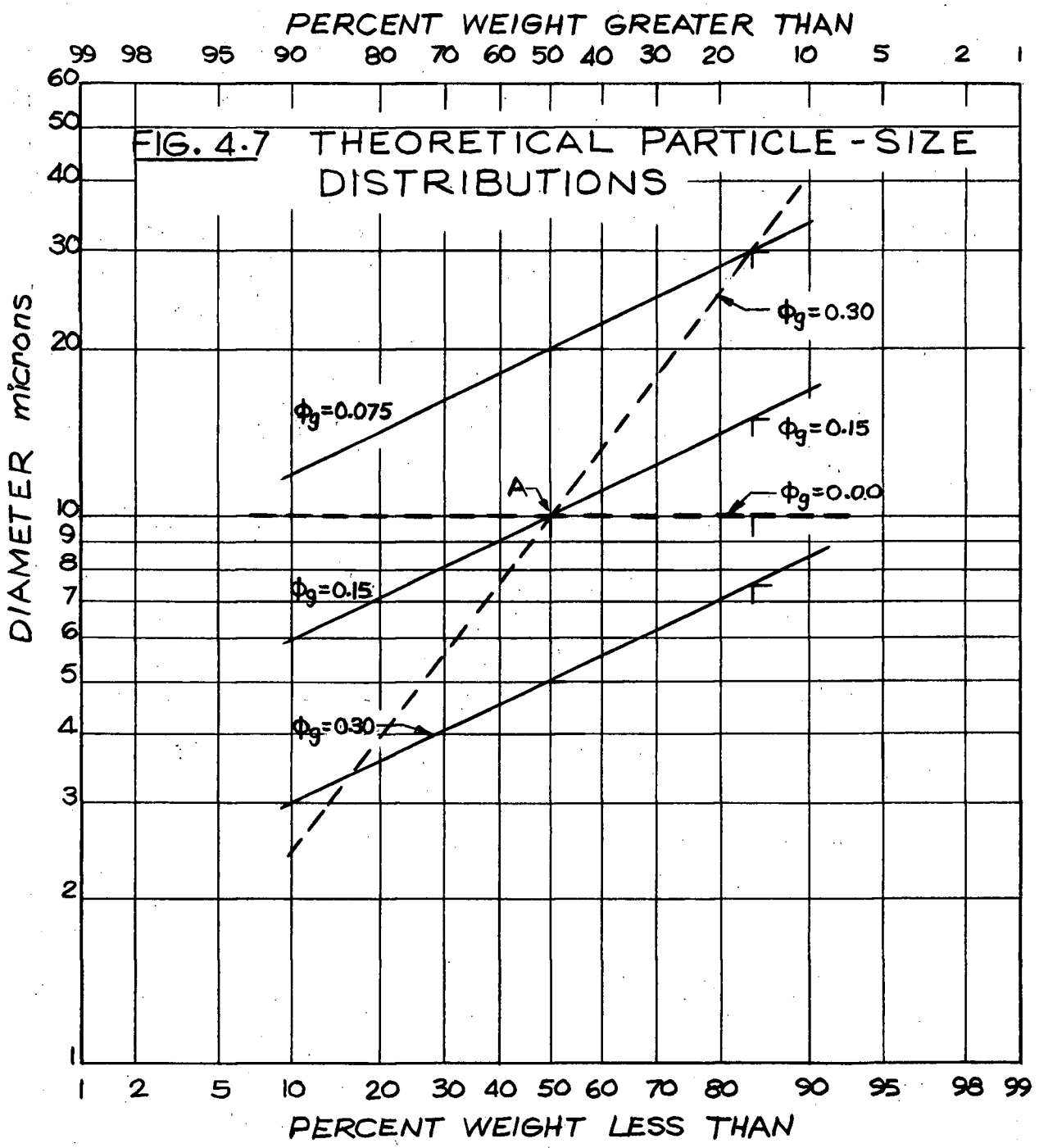

FIG. 4.7 THEORETICAL PARTICLE-SIZE DISTRIBUTIONS

the distribution with the smallest geometric mean, $\overline{d}_g$ to yield the highest penetration, as explained in the dust collector theory.

The three middle curves of Figure 4.7 illustrate three different distributions having identical geometric means but different geometric deviations. As the distribution curve is rotated counter-clockwise about point A, it is evident that as ϕ_g increases, the percentage of fines less than a given size (say 6 microns) tends to increase. Since the collector operates by inertial and centrifugal action, both of which are less effective on the smaller particles, an increase in ϕ_g would again be expected to result in an increase in π. In the case of the two curves of Figure 4.7 having $\phi_g = 0.30$ we could expect the two distributions to have similar penetrations (according to Equation 4.5) since the curve with the largest $\overline{d}_g$ also has the greatest percentage of fines below a certain size (3 microns in this case).

Thus the collector penetration depends on both $\overline{d}_g$ and s_g and cannot be correlated on the basis of particle size only. For a log-normal distribution, ϕ_g appears to be the proper correlating property.

Since the data show no trend in penetration with particle specific gravity, the specific gravity of the test dust was not considered in the correlation equation, Equation (4.5). Data taken by Semrau (15) in his correlation of penetration with expended energy across the collector show that particle density does not appear to influence the penetration. Perhaps this is due to the fact that the dust velocity is different from the nozzle velocity used in the correlation. Perhaps denser dusts, which should collect better because of their greater inertia, have less conveying velocity than the less dense dusts and hence the effect of particle weight could cancel out.

4.3.3 PARTICLE SHAPE

Particle shape has not been considered in this thesis. All particle-size distributions have been determined by the same method, sedimentation. Thus, shape factors serving as proportionality factors between particle size determination results by different methods are not required. Shape factors are also used as conversion factors for expressing results in terms of an 'equivalent sphere'. Since a sphere has the smallest surface area for a given volume, from which the 'equivalent diameter' is calculated, it falls at the highest speed. Thus an actual particle is always smaller than the 'equivalent sphere' - how much smaller will depend on the particle shape.

Experiments have shown (8) that non-spherical particles with 3 mutually perpendicular planes of symmetry will fall at very much the same velocity as spheres of the same density and volume. For the extreme case of thin laminae, the particles tend to fall edge-wise, unless disturbed by the slightest convective effects, so that they fall with their least resistance to motion. It has been found (8) that the corrections necessary to Stokes Law are usually small but should be borne in mind in the case of particles having great extensions in one or two directions.

Should a correction factor study be eventually made with the dusts used in this presentation, the correct value of ϕ_g can be found by applying the correction factor to ϕ_g directly, since s_g remains the same regardless of any change in d_i brought about by multiplication.

APPENDIX A

Solution to the Navier-Stokes Equations for the Flow of a Viscous Fluid Around a Sphere. (17)

The equations of motion for an incompressible fluid having a Reynolds number much less than unity (i.e., neglecting inertia terms) and with zero acceleration are

$$\frac{\partial P}{\partial x} = \mu \nabla^2 u$$
$$\frac{\partial P}{\partial y} = \mu \nabla^2 v$$
$$\frac{\partial P}{\partial z} = \mu \nabla^2 w \qquad (1)$$

and the continuity equation is

$$\nabla \cdot \bar{V} = 0 \qquad (2)$$

Consider uniform flow with velocity U past a sphere of radius 'a' having the coordinate system as shown below where q_r and q are the radial and tangential components of velocity at any point (r, θ).

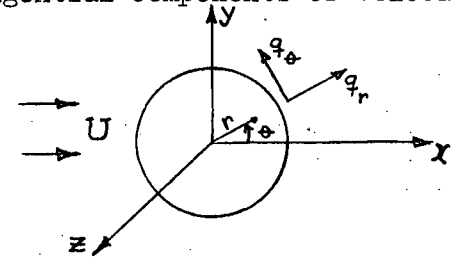

$$r^2 = x^2 + y^2 + z^2$$

The boundary conditions are:

(1) $u = v = w = 0$ at boundary for $r = a$, where u, v, and w are the x, y, and z components of velocity.

(2) $v = w = 0$ and $u = U$ when $r = \infty$

The solutions to equations (1) and (2) under the boundary conditions shown are (17).

$$u = U\left[\frac{3}{4}\frac{ax^2}{r^3}\left(\frac{a^2}{r^2}-1\right)+1-\frac{a}{4r}\left(3+\frac{a^2}{r^2}\right)\right]$$

$$v = U\frac{3}{4}\frac{axy}{r^3}\left(\frac{a^2}{r^2}-1\right)$$

$$w = U\frac{3}{4}\frac{axz}{r^3}\left(\frac{a^2}{r^2}-1\right)$$

$$p = -\frac{3}{2}\mu\frac{Uax}{r^3}\,. \qquad (3)$$

The total drag is made up of pressure drag plus shear drag.

$$D_T = D_P + D_S$$

Now $$D_P = \int_0^{\pi} -p\cos\theta \cdot dA$$

over the surface where $dA = 2\pi a \sin\theta \cdot d\theta$

so that $$D_P = 2\pi a^2 \int_0^{\pi} -p \sin\theta\cos\theta \cdot d\theta$$

Substituting the expression for p from Equation (3) for r = a, and integrating,

$$D_P = 2\pi a \mu U$$

which is the drag due to pressure.

To determine the drag due to shear, the shear stress must be found since

$$D_S = \int_0^{\pi} -\tau_{r,\theta} \sin\theta \cdot dA \qquad (4)$$

where $$\tau_{r,\theta} = \mu\left[\frac{\partial q_r}{\partial\theta} + \frac{\partial q_\theta}{\partial r}\right]$$

Choosing cylindrical coordinates, R, x as shown below

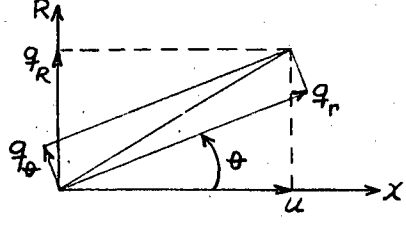

where $q_R^2 = v^2 + w^2$

then $q_\phi = q_R \cos\theta - u \sin\theta$

and q_r and q are found to be

$$q_R = \frac{3}{4} U \frac{a}{r}\left(\frac{a^2}{r^2} - 1\right) \sin\theta \cos\theta$$

$$q_\theta = -U \sin\theta \left[1 - \frac{a}{4r}\left(3 + \frac{a^2}{r^2}\right)\right]$$

and

$$\left.\frac{\partial q_\theta}{\partial r}\right|_{r=a} = -\frac{3}{2}\frac{U}{a}\sin\theta$$

and

$$\left.\frac{\partial q_r}{\partial \theta}\right|_{r=a} = 0 \text{ , since}$$

$$q_r = U\left[1 - \frac{3a}{2r} + \frac{a^3}{2r^3}\right]\cos\theta$$

Therefore

$$\tau_{r,\theta} = -\frac{3}{2}\frac{\mu U}{a}\sin\theta$$

Substituting the expression for $\tau_{r,\theta}$ into Equation (4) and integrating,

$$D_S = 4\pi a \mu U$$

The total drag is then

$$D = D_P + D_S = 6\pi a \mu U$$

Thus it is shown that two-thirds of the drag is due to shear stress and the remaining one-third is due to pressure stress.

The equation can be written as

$$D = 3\pi \mu V d$$

for a sphere of diameter d falling with a velocity V in a motionless fluid of viscosity μ.

APPENDIX B

Statistical Measures

The size parameters may be based on an assumed distribution, such as the normal distribution which ordinarily applies to symmetrical or near-symmetrical distributions about a vertical axis. The distributions of most naturally occurring fines, as well as manufactured and chemically processed fines, are asymmetrical or skewed. Sometimes the skewness may be such that the size-frequency curves become normal if the logarithm of the size is substituted for the size. In the following pages, both arithmetic and geometric parameters are calculated for the dust samples.

A histogram is drawn from the w% versus d distribution curve such that the area under the histogram is equal to 100%. The area under the histogram from say d_1 to d_2 is equal to the difference in the corresponding ordinates w_1 and w_2 for the w% versus d curve. About 15 class intervals are chosen to make up the histogram.

B-1 Calculation of Statistical Parameters

(1) Arithmetic Mean, $\bar{d}$

The arithmetic mean is given by the relation

$$\bar{d} = \frac{1}{100} \sum d_i w_i \qquad (1)$$

where

d_i = class mark on mid point of i^{th} interval

w_i = frequency in i^{th} interval, the sum of such frequencies being 100 percent.

(2) Standard Deviation, s

The standard deviation is given by the relation

$$s = \sqrt{\frac{1}{100} \sum (d_i - \bar{d})^2 w_i}$$

The variance is equal to the term inside the square root sign.

(3) Mode, m

The mode is defined as the class mark having the greatest frequency. It is the most commonly occurring value.

(4) Asymmetry Parameter, A

A measure of the departure from the normal-probability curve is given as

$$A = \frac{\bar{d} - m}{s}$$

which is zero for normal distributions and ~~negative~~ positive for distributions which are skewed to the left.

(5) Median, M

The median is the diameter for which 50 percent of the particles are less than or greater than the stated size. It is a measure of central tendency.

(6) Upper and Lower Quartiles

The upper quartile is the diameter above which 25 percent of the population falls. The value of the diameter below which 25 percent of of the population falls is called the lower quartile.

The upper and lower quartiles, as well as the median, combine to give a better physical picture of a distribution than do the mean and standard deviation.

(7) Interquartile Range

The difference between the upper and lower quartiles is called the interquartile range. It makes a good measure of dispersion and tells us the range of variability which is sufficient to contain 50 percent of the population.

(8) The 5% - 95% Range

The difference between the 95 percent less than size and the 5 percent less than size could be called a 5 percent to 95 percent Range in that it gives the range of sizes which contain the middle 90 percent of the population.

(9) Skewness Parameter, S

The ratio of the upper 45 percent range to the lower 45 percent range is a good measure of skewness or asymmetry of histograms. The ratio is unity for normal distributions and increases in value as the skewness becomes more ~~negative~~ positive, i.e. as the histogram leans more towards the left as shown below.

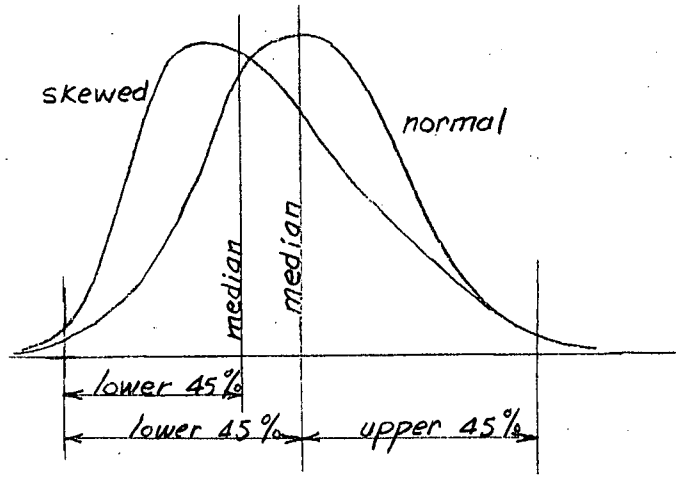

(10) Coefficient of Variation, ϕ

The ratio of the standard deviation to the arithmetic mean is called the coefficient of variation, given by

$$\phi = \frac{s}{\bar{d}}$$

The coefficient of variation is used to determine the relative variability of a distribution (6).

As an example, a distribution having mean $\bar{d} = 8$, standard deviation $s = 2$, and $\phi = 4$ is more variable than one having $\bar{d} = 9$, $s = 3$, and $\phi = 3$ which has a greater mean and a greater deviation.

The Frequency Curve

The equation of the normal-probability or frequency curve as applied to particle size is

$$F(d) = \frac{100}{s\sqrt{2\pi}} \exp. \left[- \frac{(d_i - \bar{d})^2}{2s^2} \right]$$

The constants $\bar{d}$ and s completely define the frequency function in this case.

Since nearly all particle size distributions are ~~negatively~~ positively skewed, we can make such a distribution more normal by plotting size logarithmically. In other words, most particle size distributions are covered by a normal probability equation with a logarithmic variate. Thus the equation of the log-normal frequency curve is

$$f(d) = \frac{100}{lg\, s_g \sqrt{2\pi}} \exp. \left[- \frac{(lg\, d_i - lg\, \bar{d}_g)^2}{2\, lg^2 s_g} \right]$$

where $\bar{d}_g$ is the geometric mean and s_g is the geometric deviation.

(11) Geometric Mean, $\bar{d}_g$

The geometric mean is given by

$$\lg \bar{d}_g = \frac{1}{100} \sum w_i \lg d_i$$

The geometric mean represents the value with the greatest number of particles for a log-normal distribution and therefore is better suited than the arithmetic mean. For non log-normal distributions skewed to the left, $\bar{d}_g$ is closer to the median than $\bar{d}$ is since $\bar{d}_g$ is always less than $\bar{d}$.

(12) Geometric Deviation, s_g

The geometric deviation is given by

$$\lg s_g = \sqrt{\frac{1}{100} \sum (\lg d_i - \lg \bar{d}_g)^2 w_i}$$

The geometric mean and geometric deviation are to log-normal distributions as the arithmetic mean and standard deviation are to normal or Gaussian distributions.

(13) Geometric Coefficient of Variation, ϕ_g

Similarly as in the normal case, the geometric coefficient of variation is defined to be

$$\phi_g = \frac{s_g}{\bar{d}_g}$$

As in the normal case, ϕ_g is a relative measure of variation. It tends to be much less than unity for very narrow distributions and increases with increasing spread.

B-2 Graphical Determination of Mean and Deviation (4)

An important property of size distributions (w versus d) having normal frequency functions is that the mean is equal to the median (50 percent size) and the standard deviation is given by

$$s = 84.13\% \text{ size} - 50 \text{ percent size}$$

$$= 50 \text{ percent size} - 15.87\% \text{size}$$

This is because the probability integral defines that 68.26 percent of the total distribution lies between $(\bar{d} + s, \bar{d} - s)$.

When such distributions are plotted on an arithmetic-probability grid, a straight line results and the mean and deviation can thus be determined quite readily.

Similarly when log-normal distributions are plotted on a log-probability grid, a straight line results, the geometric mean being equal to the 50 percent size and the geometric deviation given by

$$s_g = \frac{84.13\% \text{ size}}{50\% \text{ size}} .$$

It can be seen that ϕ_g for a log-normal distribution can be given by

$$\phi_g = \frac{s_g}{\bar{d}_g} = \frac{84.13\% \text{ size}}{(50\% \text{ size})^2}$$

B-3 Replication of Data (5)

The mean of two size distributions from the same population is given by

$$\bar{d} = \frac{n_1\bar{d}_1 + n_2\bar{d}_2}{n_1 + n_2}$$

where n_1 and n_2 are the sizes of the two random samples making up the distributions.

The standard deviation of the two size distributions is given by

$$s = \left[\frac{n_1 s_1 + n_2 s_2^2}{n_1 + n_2} + \frac{n_1 n_2 (\bar{d}_1 - \bar{d}_2)^2}{(n_1 + n_2)^2}\right]^{\frac{1}{2}}$$

BIBLIOGRAPHY

1. Dallavalle, J.M., "Micromeritics", New York, Pitman Publishing Corporation, 1943

2. Orr, C., Dallavalle, J.M., "Fine Particle Measurement", New York, The MacMillan Company, 1959.

3. Cadle, R.D., "Particle Size Determination", New York, Interscience Publishers, Inc., 1955.

4. Zenz, F.A., Othner, D.F., "Fluidization and Fluid Particle Systems", New York, Reinhold Publishing Corp., 1960.

5. Hoel, P.G., "Introduction to Mathematical Statistics", New York, John Wiley & Sons Inc., 1960.

6. Moroney, M.J., "Facts From Figures", Baltimore, Penguin Books Inc., 1956.

7. Schenck, H, Jr., "Theories of Engineering Experimentation", New York, McGraw-Hill Book Co., 1961.

8. Herdan, G., "Small Particle Statistics", London, Butterworths, 1960.

9. Wilson,Bright, E, Jr., "An Introduction to Scientific Research", New York, McGraw-Hill Book Co., 1952.

10. Lapple, C.E., "Fluid and Particle Mechanics", University of Delaware, Newark, Delaware, 1954.

11. Bostock, W., "A Sedimentation Balance for Particle Size Analysis in the Sub-sieve Range", J. Sci. Instrum., Vol.29, 1952, p.209.

12. Cohen, L., "A Sedimentation Balance for Particle Size Analysis", Instrum. Pract., Oct., 1959.

13. Jarrett, B.A., Heywood, H., "A Comparison of Methods for Particle Size Analysis", Brit. J. App. Phy., Supp. No.3, p.S21, 1954.

14. Heywood, H., "Techniques for the Evaluation of Powders", Powder Metallurgy, No.7, 1961.

15. Semrau, K.T., et al., "Influence of Power Input on Efficiency of Dust Scrubbers", Ind. Eng. Chem., V.50, p.1615, Nov., 1958.

16. Wighton, J.L., "The Fundamental Variables Affecting the Operation of a Wet-Type Dust Collector", Ph.D. Thesis, University of Michigan, 1955.

17. Lamb, H., "Hydrodynamics", New York, Dover Publications, 1932.

18. Stearns, et al., "Flow Measurement with Orifice Meters"